DOI: 10.1002/ ((please add manuscript number))

Article type: Full Paper

N-Acetylgalactosamine-targeted delivery of dendrimer-doxorubicin conjugates influences doxorubicin cytotoxicity and metabolic profile in hepatic cancer cells

*Sibu P. Kuruvilla[+], Gopinath Tiruchinapally[+], Mahmoud ElAzzouny, Mohamed E.H. ElSayed**

[+]These authors contributed equally to this research work.

S. P. Kuruvilla

University of Michigan

Department of Materials Science and Engineering

2300 Hayward St.,

Ann Arbor, MI 48109, USA

G. Tiruchinapally, Ph.D.

Research Scientist

University of Michigan

Department of Biomedical Engineering

1101 Beal Avenue

Ann Arbor, MI 48109 , USA

M. ElAzzouny, Ph.D

Research Investigator

University of Michigan Medical School

Department of Internal Medicine

1500 East Medical Center Drive

Ann Arbor, MI 48109, USA

Associate Professor M. E.H. ElSayed, Ph.D.

University of Michigan

Department of Biomedical Engineering

1101 Beal Avenue

Ann Arbor, MI 48109 , USA

(and)

Department of Macromolecular Science and Engineering

2300 Hayward Avenue

Ann Arbor, MI 48109, USA

melsayed@umich.edu

Keywords: PAMAM dendrimers, aromatic azo-linkers, N-acetylgalactosamine ligands, hepatocellular carcinoma, metabolomics

This study describes the development of N-acetylgalactosamine (NAcGal)-targeted, doxorubicin (DOX)-loaded, generation 5 (G5) poly-amidoamine dendrimers able to achieve cell-specific delivery and release of DOX into the cytoplasm of hepatic cancer cells. G5 is functionalized with 16.6 PEG brushes displaying NAcGal ligands to target hepatic cancer cells. DOX is conjugated to G5 via two aromatic azo-linkages, L3 and L4, to achieve tunable hepatic cancer cell-specific release of the drug. The combination of PEGylated NAcGal ligands with similar loading of L3-DOX and L4-DOX resulted in P1 ((NAcGal$_{\beta}$-PEG*c*)$_{16.6}$-G5-(L3-DOX)$_{11.6}$) and P2 ((NAcGal$_{\beta}$-PEG*c*)$_{16.6}$-G5-(L4-DOX)$_{13.4}$) conjugates, respectively. After confirming the conjugates' biocompatibility, flow cytometry studies show P1 and P2 achieve 100% uptake into hepatic cancer cells at 30-60 nM particle concentration. This internalization correlated with cytotoxic activity against HepG2 cells with IC_{50} values of 24.8, 1,414.0 and 237.8 nM for free DOX, P1, and P2, respectively. Differences in cytotoxic activity prompted the use of metabolomics to identify the intracellular release behavior of DOX. While treatment with free DOX results in intracellular delivery of two expected DOX metabolites, P1 and P2 conjugates release two alternative DOX metabolites, namely tetracenomycin-like analogues. The different metabolites induce different effects on metabolic cycles, as seen in studies using stable isotope tracers. Namely, free DOX significantly reduces glycolysis and increases fatty acid oxidation, while P1 and P2 conjugates increase glycolysis, likely as a response to high oxidative stress. Overall, P1 and P2 conjugates exhibit high potential as a platform drug delivery technology for improvement of hepatic cancer therapy.

1. Introduction

Hepatocellular carcinoma (HCC) is the 5th most commonly-occurring cancer worldwide and the 2nd highest cause for cancer-related deaths globally.[1,2] The poor prognosis and treatment of HCC is highlighted by the 782,000 new cases that developed in 2012 and the 746,000 deaths that resulted from it in the same year[2] leading to a global mortality-to-incidence ratio of 0.95.[1–3] In the US, the incidence rate of HCC has more than doubled in the last three decades and is anticipated to reach peak incidence rates before 2030,[4,5] which emphasizes the need to develop an effective therapeutic strategy.

Currently, the most common therapeutic strategy is the direct injection of chemotherapeutic agents (e.g. doxorubicin, DOX) into the hepatic artery through a process called hepatic arterial infusion (HAI).[6] A common modification of this procedure is the co-delivery of an embolizing agent to restrict arterial bloodflow and induce ischemia in addition to the chemotherapeutic effect of DOX, a technique called transarterial chemoembolization (TACE).[7–9] Unfortunately, HAI and TACE are severely hindered by high complication rates such as dose-limiting toxicities (e.g. cardiotoxicity, myelosuppression, and hepatic failure),[10] high rates of tumor recurrence, and development of chemoresistance.[7,11–13] Off-target toxicity arises mainly from the leakage of DOX into the systemic circulation leading to the unintended delivery of DOX to surrounding healthy tissue,[10,14] while chemoresistance develops through upregulation of drug efflux pumps in response to xenobiotic compounds such as DOX.[15]

Our strategy to address the limitations of HAI/TACE and the associated systemic toxicity of the administered chemotherapeutic agent is to engineer a targeted polymer-drug conjugate that can accumulate in the tumor tissue upon parenteral administration, get internalized by hepatic cancer cells via receptor-mediated endocytosis, and achieve selective release of the loaded chemotherapeutic cargo to trigger cancer cell death. Specifically, we utilize generation 5 (G5) of poly-amidoamine (PAMAM) dendrimers as the core carrier for DOX (as a model chemotherapeutic drug) and *N*-acetylgalactosamine (NAcGal) as a targeting ligand for hepatic cancer cells. G5 poly-amidoamine dendrimers are water-soluble, spherical polymers that have 128 terminal amine groups, allowing the functionalization of the surface with compounds like drugs, imaging agents, or genetic material.[16,17] We recently reported that G5 dendrimers displaying NAcGal ligands in the beta-conformation ($NAcGal_{\beta}$) on the end of a 2 kDa poly(ethylene glycol) (PEG) brush and attached to the G5 surface via an acid-labile cis-aconitic (*c*) linkage were able to achieve selective internalization into hepatic cancer cells.[18,19] These $NAcGal_{\beta}$-PEG*c*-G5 conjugates escaped recognition by healthy hepatocytes and liver macrophages[18,19] by targeting the asialoglycoprotein receptor (ASGPR) overexpressed on hepatic cancer cells.[20,21] Upon internalization via receptor-mediated endocytosis, the cis-aconityl linkages are hydrolyzed in the acidic endosomes resulting in the shedding of the PEG brush and release of the G5 carrier into the cytoplasm via their endosomolytic activity mediated by the proton sponge effect.[22] We reported the synthesis of aromatic azo-benzene linkers that incorporate a 1,6 self-eliminating electron cascade and utilized them to conjugate DOX to G5 dendrimers.[23] These aromatic azo-benzene linkers are substrates for azoreductase enzymes expressed by hepatic cancer cells, which mediates cancer cell-specific release of the conjugated cargo.[23] We showed that changing the electron density surrounding the azo-linkage [L(x)] by

modifying the substituents in X and Y positions allows us to modulate the affinity to azoreductase enzymes, tune DOX release, and impact the associated cytotoxicity.[23] Namely, the L3 (X: N-CH_3; Y: H) and L4 (X: N-CH_3; Y: O-CH_3) linkages exhibited amenable DOX release profiles that correlated with anticancer activity comparable to the toxicity of free DOX in hepatic cancer cells.[23]

In this manuscript, we successfully conjugated DOX to G5 dendrimers via aromatic azo-linkers and grafted NAcGal$_\beta$-PEG via acid-labile cis-aconityl linkages to prepare two targeted G5-DOX nano-conjugates. We conjugated DOX to G5 dendrimers via L3 and L4 aromatic azo-linkers and attached NAcGal$_\beta$-PEG*c* chains to the G5 dendrimers to prepare **P0** [(NAcGal$_\beta$-PEG*c*)$_{12.1}$-G5], **P1** [(NAcGal$_\beta$-PEG*c*)$_{16.6}$-G5-(L3-DOX)$_{11.6}$], and **P2** [(NAcGal$_\beta$-PEG*c*)$_{16.6}$-G5-(L4-DOX)$_{13.4}$] (**Figure 1**). We investigated their biocompatibility to determine their potential as an intravenous therapy by quantifying their induction of hemolysis, platelet aggregation, and opsonization by serum proteins. We investigated their uptake by hepatic cancer cells, and the associated anticancer activity compared to free DOX. Prompted by the observed difference in cytotoxicity of free DOX compared to P1 and P2, we employed metabolomics to quantify DOX release and identify the species released from P1 and P2 inside the cytoplasm. This investigation revealed a difference in intracellular species of DOX delivered by the three treatments, as well as a difference in the induced metabolic response (e.g. glycolysis, fatty acid oxidation, and tricarboxylic acid (TCA) cycle), as measured by targeted and untargeted metabolomics approaches. Insights into the efficacy of P1 and P2 conjugates will help evaluate their potential as a platform technology and as an alternative therapy for hepatocellular carcinoma in the clinic.

2. Results and Discussion

2.1. Synthesis and Characterization of P1 and P2 Conjugates

We synthesized G5 dendrimers functionalized with both NAcGal$_\beta$-PEG*c* targeting moieties as well as *L*(x)-DOX linkages by combining our previous synthetic methodologies[18,23] with minor modifications (**Figure 2**). We confirmed that conjugation of 16.6 NAcGal$_\beta$-PEG*c* units onto G5 surface by NMR and MALDI-TOF (**Figure S1**). This corresponds to 13.0 mole% PEGylation of the dendrimer surface, which provides sufficient packing (>5 mol%) to trigger PEG chains to adopt a "brush" conformation instead of the "mushroom" regime.[24,25] This brush conformation enables PEG chains to completely cover the particle's surface and shield it from non-specific adsorption of serum proteins, which mediates the particle's clearance by the reticuloendothelial system (RES) (i.e. liver, lungs, spleen).[24–26]

The PEGylated G5 (compound **11**) was coupled with L3-DOX or L4-DOX conjugates via click chemistry following published protocols.[23] Starting with the same precursor molecule (compound **11**) ensured equal density of NAcGal targeting ligands per G5 particle before loading of the chemotherapeutic agent (DOX). We achieved similar DOX loading in P1 (compound **12**) [(NAcGal-PEG*c*)$_{16.6}$-G5-(L3-DOX)$_{11.6}$] conjugates and P2 (compound 13) [(NAcGal-PEG*c*)$_{16.6}$-G5-(L4-DOX)$_{13.4}$] reaching 11.6 moles and 13.4 moles per G5, respectively (**Figure 2**). We previously established that loading of 16 DOX molecules per G5 (i.e. 12.5 functionalization of surface amine groups) is the maximum capacity to maintain the

aqueous solubility of G5-DOX conjugates.[23] Similarly, P1 and P2 conjugates exhibited intrinsic aqueous solubility at concentrations up to 1.25 mg/mL.

We measured the size of our conjugates using dynamic light scattering (DLS), identifying that P1 and P2 have hydrodynamic diameters (HD) of 6.02 ± 0.28 nm and 6.39 ± 0.40 nm, respectively (**Table 1**). This size places P1 and P2 conjugates in the ideal size range that will enable them to surpass renal filtration from the blood (HD < 5nm[27,28]), and thus extends their circulation time within the bloodstream. We also measured the particle size of acetylated G5 (G5-$(Ac)_{128}$) and non-DOX-loaded P0 conjugates to be used as controls (**Table 1**). We measured the molecular weights of P1 and P2 using MALDI-TOF, which are 84,572 and 85,553 Da, respectively (**Table 1; Figure S2 and S3**). This range of MWs places P1 and P2 conjugates well above the molecular weight cut-off of 40 kDa required to escape renal clearance. This MW range also allows them to exploit the enhanced permeation and retention (EPR) effect,[29–32] indicating that during circulation they can extravasate into the tumor interstitium due to its leaky vasculature and be retained there due to the lack of a proper lymphatic drainage system. Finally, we measured the zeta potential of P1 and P2 conjugates which were -0.63 ± 0.28 mV and -0.46 ± 0.23 mV, respectively. The neutral surface charge is important to ensure biocompatibility of PAMAM dendrimers,[33] and also guarantees that the internalization mechanism into cells will not be jeopardized by non-specific charge-charge interactions.[34]

2.2. Biocompatibility of P1 and P2 Conjugates

We measured the extent of hemolysis induced by P1 and P2 conjugates in the presence of freshly isolated red blood cells (RBCs) by quantifying the amount of released hemoglobin from ruptured RBCs after a 1 hour incubation at 37 ºC, and compared this behavior to naked, non-PEGylated G5-$(NH_2)_{128}$ dendrimers (**Figure 3, Panel A**). Results are presented as a percentage of hemolysis caused by distilled (DI) water, which is considered to cause 100% hemolysis through osmotic swelling and rupture of RBCs.[35] Unmodified G5-$(NH_2)_{128}$ dendrimers exhibited complete hemolysis (98.7 ± 3.1%), which can be attributed to membrane destabilization caused by the cationic quaternary ammonium ions that develop at the amine-terminated surfaces of PAMAM dendrimers.[36,37] In comparison, P1 and P2 completely suppressed hemolysis, verifying the established ability of nanoparticle PEGylation[38–40] and neutral surface charge[41] to prevent membrane destabilization and rupture of RBCs.

To ensure both P1 and P2 do not induce platelet aggregation in the bloodstream, we used light transmission aggregometry to measure the activation of platelets in the presence of either particle, following published protocols[42] (**Figure 3, Panel B**). After drawing fresh blood and isolating the platelet rich plasma (PRP) and platelet poor plasma (PPP) fractions, we added either P1 or P2 to the PRP fraction and compared the resulting aggregation over 10 minutes to that caused by naked G5-$(NH_2)_{128}$ dendrimers or P0 conjugates at an equivalent G5 concentration. Results show that the positive control of adenosine diphosphate (ADP) caused the highest amount of platelet aggregation (26.3 ± 5.36%), which is not surprising due to its established role in platelet activation.[43,44] The effect of PEGylation and surface charge

of G5 dendrimers is evident when comparing the 9% platelet aggregation caused by unmodified, cationic G5-$(NH_2)_{128}$ dendrimers versus the 0% aggregation caused by the PEGylated P0 particle. Importantly, P1 and P2 conjugates induced no platelet aggregation, indicating that despite the addition of L(x)-DOX molecules (thereby imparting hydrophobicity to the P0 skeleton), PEGylation takes precedence and is able to protect the conjugates from activating platelets.

The advantage of PEGylation and its precedence over the addition of hydrophobic L(x)-DOX linkages is further evident in the opsonization of P1 and P2 conjugates. Opsonization, or the fouling of a surface by nonspecific protein adsorption during plasma circulation, leads to rapid shuttling of nanoparticles to organs of the RES within minutes of intravenous delivery. As such, opsonization is one of the largest barriers facing nanomedicine strategies.[45–47] To approximate the extent of opsonization of our NP formulations, we measured the binding of bovine serum albumin (BSA) to their surfaces using the change in intrinsic fluorescence of BSA, which is quenched when the protein binds to the NP surface.[18] In particular, we investigated the adsorption of BSA to P1 and P2 conjugates in comparison to G5-$(NH_2)_{128}$ dendrimers and P0 conjugates at equal G5 concentration (**Figure 3, Panel C**). Results show that the fluorescence intensity of free BSA remained relatively unchanged during the 60-minute incubation period and thus was used as the negative control. Cationic, G5-$(NH_2)_{128}$ dendrimers exhibit high (4-7 folds) fluorescence quenching, reaching an I^0/I value of 7.18 ± 1.90 at the end of the incubation period. This is expected given the high surface charge of the particle due to the 128 free terminal amines on its surface. In comparison, P0 conjugates

exhibit no fluorescence quenching, which is not surprising given its neutral surface charge imparted by the capping (acetylation) of the free amine groups as well as the hydrophilic nature of the PEG that is able to prevent protein adsorption to the particle surface.[18] As mentioned, neither P1 nor P2 conjugates exhibited any fluorescence quenching, suggesting that they are able to escape recognition by serum proteins. Moreover, P1 and P2 conjugates have free amines that are not acetylated nor functionalized, yet the 16.6 moles of 2 kDa PEG chains with hydrophilic NAcGal$_\beta$ ligands are able to cover their surfaces and mask them from protein recognition.

Taken together, the high *in vitro* biocompatibility observed in these results validates the utility of PEGylation, water-soluble polymers, neutral surface charge, and functionalization with hydrophilic NAcGal$_\beta$ targeting ligands for intravenous drug delivery systems. Results suggest that P1 and P2 conjugates will be able to overcome rapid clearance from the bloodstream and can be retained long enough in circulation to exploit the EPR effect and achieve high intratumoral concentrations, all while causing minimal adverse effects to blood components.

2.3. Uptake of P1 and P2 conjugates into hepatic cancer cells

We were interested to see if the addition of L(x)-DOX molecules to NAcGal$_\beta$-targeted, PEGylated G5 dendrimers would be able to retain affinity for hepatic cancer cells. Therefore, we measured the internalization of P1 and P2 conjugates into HepG2 or Hep3B cells over 2 and 24 hours as a function

of concentration via flow cytometry. We previously established that the ideal concentration range of $NAcGal_{\beta}$ ligands is 10-4000 nM in order to achieve controllable labeling and internalization of G5-based conjugates into HepG2 and Hep3B cells.[18] Therefore, we incubated P1 and P2 conjugates over this $NAcGal_{\beta}$ concentration range, which is equal to 0.6-240 nM of P1/P2 conjugates. We used the intrinsic fluorescence of DOX to measure the number of cells labeled by P1/P2 conjugates and we included equivalent concentrations of free DOX to compare the internalization of free DOX to that delivered by G5 carriers. It is important to note that we accounted for the slight difference in DOX-loading in P1 and P2 by adjusting the concentration of free DOX used in uptake studies to allow accurate assessment of the particle's internalization (**Figure 4**).

Results show P1 and P2 conjugates are internalized into hepatic cancer cells in a concentration-dependent manner, which is higher than the internalization of equivalent concentrations of free DOX (**Figure 4, Panels A & C**). In HepG2 cells, at a $NAcGal_{\beta}$ concentration of 100 nM, P1 conjugates fluorescently-label 14% of cells and P2 conjugates label 39% (**Figure 4, Panel A**). Free DOX, on the other hand, at both equivalent concentrations (46 nM DOX for P1, or 61 nM for P2) only labels 2% of HepG2 cells. As the $NAcGal_{\beta}$ concentration increased to 500 nM, P2 conjugates virtually label all cells, while free DOX only labels 2%. Similarly, P1 reaches 97% labeling of cells at a $NAcGal_{\beta}$ concentration of 1000 nM, while the equivalent incubation of free DOX only labels 43% of cells. At the highest concentration of 4000 nM, all formulations reach 100% cell labeling. Similarly, P1 conjugates fluorescently-labeled up to 12-folds more Hep3B cells than free DOX and P2 labeled up to 78-folds more cells (**Figure 4, Panel C**). We also investigated the uptake of P1 and P2 conjugates into a control cell line, SK-Hep1, which is ASGPR-deficient.[48–50] Results show that these cells do not bind

or internalize P1/P2 conjugates, demonstrating that uptake of the conjugates into HepG2 and Hep3B cells is ASGPR-mediated (**Figure S4**). Further, we normalized the relative fluorescence intensity of fluorescently-labeled HepG2 and Hep3B cells to that of untreated cells in order to measure the difference of intracellular DOX concentration between different formulations (**Figure 4, Panels B & D**).[18,51,52] P1 and P2 conjugates achieved up to 6-folds increase in intracellular DOX concentration over the free drug incubation in HepG2 cells (**Figure 4, Panel B**). In Hep3B cells, P1 achieved up to 4-folds increase over free DOX while P2 achieved a 19-fold increase at the highest particle concentration (**Figure 4, Panel D**).

These results indicate that the higher fluorescent labeling and intracellular fluorescence of DOX mediated by P1 and P2 conjugates in both HepG2 and Hep3B cells highlights the advantage of active targeting through $NAcGal_{\beta}$-facilitated receptor endocytosis. We previously established that the display of $NAcGal_{\beta}$ ligands at the end of a PEG brush was able to achieve selective internalization of G5 dendrimers into hepatic cancer cells, and escaped recognition by non-target cells, namely healthy hepatocytes and liver macrophages (i.e. Kupffer cells).[18] It is evident that P1 and P2 conjugates maintain uptake capability into hepatic cancer cells, despite the addition of L(x)-DOX molecules, and in terms of percentage of cells labeled and intracellular DOX fluorescence, they exhibit a clear advantage over passive diffusion of free DOX. In addition, it is important to note that P1 and P2 conjugates exhibit higher cell labeling and higher intracellular concentration in Hep3B cells than HepG2 cells almost universally, achieving a maximum of 5.4-folds higher intracellular fluorescence for P2 conjugates at the same concentration (**Figure 4, Panels B and D**). We attribute this differential

to the variation in expression of ASGPR between cell lines, which has been confirmed to be greater for Hep3B cells than in HepG2 cells.[20,53,54]

2.4. Cytotoxic Activity of P1 and P2 conjugates

We incubated free DOX, P1, and P2 conjugates with HepG2 and Hep3B cells over 72 hours and used the clonogenic survival assay to measure cell survival following our published protocols.[23] As expected, free DOX induced an exponential decrease in HepG2 cell survival with increasing DOX concentration, achieving an IC_{50} (median concentration of drug required to inhibit cell growth by 50%) of 24.8 ± 1.2 nM (**Figure 5, Panel A**). This IC_{50} is comparable to our established results and falls in the expected range of DOX toxicity in HepG2 cells for these treatment conditions.[55,56] We measured the intrinsic toxicity of P0 and results show that it has insignificant toxicity within the investigated concentration range with IC_{50} > 10,000 nM (**Figure 5, Panel A**). P1 and P2 conjugates exhibited increasing toxicity with increasing DOX concentration achieving IC_{50} values of 1414.0 ± 1.4 and 237.8 ± 1.2 nM, respectively (**Figure 5, Panel A**). It is evident that P2 has a higher activity than P1 indicated by its IC_{50} value that is 6-folds lower than that of P1. This is expected given that it has 1.8 more DOX moles/G5 carrier and the higher affinity for azoreductase enzymes responsible for cleavage of the linkage and release of DOX as established in previous reports.[23] Results in Hep3B cells follow similar trends (**Figure 5, Panel B**) with toxicity increasing exponentially with DOX concentration, while the carrier P0 again shows insignificant toxicity with an IC_{50} ~ 10,000 nM (**Figure 5, Panel B**). Consistent with previous results,[23,55] Hep3B cells are more sensitive to treatment than HepG2 cells, with free DOX, P1, and P2 having lower IC_{50} values of 18.6 ± 1.3, 78.5 ± 1.1, and 145.5 ±

1.25 nM, respectively. In addition to the higher intrinsic sensitivity to treatment, our internalization results (**Figure 4, Panels B and D**) also showed that P1 and P2 conjugates achieve higher intracellular concentrations in Hep3B over HepG2 cells, and thus higher intracellular DOX concentrations may be contributing to the higher toxicity. Further, similar to what we observed in our previous results,[23] P1 particles are more cytotoxic than P2 particles in Hep3B cells. We hypothesize that this variation may be attributed to differences in azoreductase identity and expression between cell lines, but further studies are required to test this hypothesis. Nevertheless, these results verify that P1 and P2 conjugates are able to exhibit toxicity towards hepatic cancer cells that is comparable to free DOX and this toxicity can be optimized by tuning linkage composition.

2.5. Intracellular release of DOX from P1 and P2 conjugates via metabolomics studies

The differences in cytotoxicity between free DOX, P1, and P2 particles prompted us to elucidate the intracellular fate of DOX being delivered by each treatment. We employed metabolomics to determine the chemical fingerprints of DOX delivered by P1 and P2 conjugates intracellularly in comparison to DOX delivered freely in solution. We chose a treatment time of 12 hours to provide a snapshot of metabolic alteration induced by the DOX-loaded conjugates without causing substantial cell death commonly observed after 24 hours.[57,58] Both intracellular and extracellular metabolites were analyzed by LC-MS (**Figure 6**). Results show that treatment of HepG2 cells for 12 hours with free DOX results in detection of the parent DOX ($[M-H]^-$: 542.1710) and 7-deoxydoxorubicinone ($[M-H]^-$: 395.0587), which is its deglycosylated form (**Figure 6, Panel A**). This conversion has been shown

to be mediated by a combination of cytochrome P450s and NADH dehydrogenase,[59,60] which are both cytosolic enzymes.

Although P1 and P2 conjugates exhibited significant cytotoxicity towards HepG2 cells (**Figure 5**), results show a significantly lower amount of the parent DOX present intracellularly from these treatments (**Figure 6, Panel A**). This can be attributed to slow release of DOX molecules from P1 and P2 conjugates, which dramatically minimized intracellular concentration of parent DOX at this 12-hour time point. Using untargeted metabolomics, we found both P1 and P2 conjugates generated two specific molecules that are structurally similar to the anthracycline backbone of DOX but only one that matched the exact mass ($[M-H]^-$: 335.0561) of a known DOX metabolite recently described by Kaushik *et al.*[61] (**Figure 6, Panel B**). These molecules are similar in exact mass to tetracenomycin (TCM) compounds, which are structural isomers of DOX metabolites[61] that are known to exhibit similar cytotoxicity via DNA intercalation, topoisomerase II inhibition, and generation of reactive oxygen species (ROS).[62–64] Therefore, we chose TCM nomenclature to identify these metabolites. However, it is important to note that TCM compounds are less potent than the parent DOX, which is indicated by their higher IC_{50} values.[63] For example, Gan *et al.* reported an IC_{50} of 7.5 µM for TCM X in HepG2 cells compared to an IC_{50} of 1.6 µM for DOX.[63] The TCM F1 methylester analogue ($[M-H]^-$: 379.0823) appeared in the intracellular extracts of P1- and P2-treated cells at similar quantities (**Figure 6, Panel B**), which indicates that this metabolite is generated from the P1/P2 conjugates by intracellular enzymes. The second and most prominent metabolite identified from P1- ad P2-treated cells is TCM D1 ($[M-H]^-$: 335.0561), which results from the loss of an acetaldehyde group from TCM F1 methylester (**Figure 6, Panel B**). Free DOX treatments also generated the TCM D1 metabolite,

which is not surprising given that it is a downstream metabolite of parent DOX after the loss of a glycoaldehyde group from 7-deoxydoxorubicinone.[61] However, the quantity of intracellular TCM D1 in free DOX-treated cells, is 9- and 4-folds lower than that observed in P1 ($P<0.05$) and P2 ($P<0.01$) treated cells, respectively (**Figure 6, Panel B**). Interestingly, the levels of TCM D1 inside HepG2 cells are significantly higher for P1 treated cells compared to those incubated with P2 ($P<0.05$) while the extracellular concentration of the same metabolite is reversed (i.e higher for P2 than P1, $P<0.01$). It is also important to note that TCM D1 molecules were generated when P1 and P2 conjugates were incubated with PBS alone (data not shown), albeit at lower levels than those detected inside HepG2 cells. This suggests that introducing the drug with a nanoparticle might force it to undergo special chemical modifications that could exert toxic effects on its own. Additionally, since it is also common to see non-specific degradation pathways for free DOX molecules in buffers,[65] it is possible that P1 and P2 conjugates are not completely devoid of this degradation either.

The exact mechanism of intracellular release and metabolism of DOX delivered by P1 and P2 conjugates that result in generation of TCM F1 and D1 molecules is still unclear. Earlier reports show that changing the enzyme responsible for releasing a therapeutic cargo from a polymer-drug conjugate leads to recognizable difference in kinetics of drug release, drug metabolism, and associated intracellular activity. For example, Greco *et al.* observed stark differences in the release and activity of DOX against breast cancer cells when singly loaded onto a HPMA polymer or loaded in combination with aminoglutethimide (AMG) due to differences in the enzymes involved in drug release between the two HPMA-DOX conjugates.[66] Similarly, we hypothesize that azoreductase enzymes responsible for DOX release from P1 and P2 conjugates may impact not only the release

kinetics but also intracellular metabolism of the released DOX molecules. Our current focus is on elucidating the mechanism of DOX intracellular release from P1 and P2 and its metabolism compared to free DOX.

2.6 Effect of P1 and P2 conjugates on HepG2 metabolic pathways

We extended our metabolomics analysis to measure the metabolic response induced by P1 and P2 conjugates compared to free DOX treatment using an untargeted metabolomics approach and also by determining relative flux using stable isotope tracers. Principle component analysis (PCA) of all features detected by untargeted analysis showed clear clustering within each treatment type and clear distinctions between each group, which indicates different metabolic profiles induced by each treatment (**Figure 7, Panel A**). Targeted analysis of major biochemical pathways such as central carbon metabolism showed clear distinctions between DOX-treated and P1/P2-treated cells (**Figure 7, Panels B and C**). **Figure 7 Panel B** identifies the differences in the presence of key markers of glycolysis and the tricarboxylic acid (TCA) cycle based on either DOX or P1/P2 treatment. Most notably, metabolites involved in glycolysis and the TCA cycle are reduced 2-4 folds in DOX-treated cells while they are almost all upregulated up to 2-folds greater in P1- and P2-treated cells. Similar metabolic changes induced by free DOX have been described before[67,68] where glycolysis was reduced as well as protein, purine, pyrimidine, and glutathione biosynthesis. The inhibition of glycolysis most probably increased the oxidation of substrates other than glucose to increase ATP generation for cell survival after DOX damage.[69] In comparison, P1 and P2 conjugates induced increases in markers of glycolysis such as fructose 1,6-bisphosphate and the TCA cycle intermediates

such as citrate (**Figure 7, Panel B**). We hypothesize that the increase in glycolysis is a response to oxidative stress caused by the generation of ROS, a primary mechanism of DOX and DOX-metabolite toxicity.[70,71] This is supported by several studies correlating increased glycolysis with oxidative stress and mitochondrial dysfunction.[72–74] Wu and Wei in their work showed increased glycolytic flux was a result of oxidative stress in skin fibroblasts from patients with myoclonic epilepsy and ragged-red fiber (MERRF) syndrome, in an attempt to generate NADH to help mitigate ROS generation.[72] Valbuena *et al.* verified the increase in glycolysis and TCA cycle was a result of poor adaptation to ROS generated in amyotrophic lateral sclerosis (ALS) neuronal cells, and was a sign of neuronal death.[73] Further, plasma from patients with Alzheimer's disease, a neurodegenerative disorder associated with increased oxidative stress, caused mitochondrial dysfunction and increased glycolysis as a compensatory action, ultimately leading to a loss of cell viability, as studied by Jayasena *et al.*[74] Therefore, our data may suggest that the delivery of TCM F1 and D1 moieties causes high oxidative stress leading to upregulation of glycolysis and the TCA cycle and may be the primary mechanism of toxicity observed with P1 and P2 conjugates. This also explains the 3- to 5-fold increase in oxidized glutathione (GSSG) present in P1/P2-treated cells (**Figure 7, Panel B**), which is normally upregulated to scavenge ROS.[71] Further examination of ROS presence and mitochondrial function will elucidate whether this is indeed the phenomenon at play.

To compensate for reduced glycolysis, it has been established that DOX-treated cells increase fatty acid oxidation upon treatment.[75] To further investigate the effect of different substrates on the relative utilization of fatty acid and glucose, we applied the stable isotope tracer strategy. We treated cells with DOX, P1, or P2 for 12 hours, followed by a 4-hour incubation with 10 mM U-^{13}C

glucose and 100 uM oleate or 10 mM unlabeled glucose with 100 uM U-^{13}C oleate. We found reduced incorporation of ^{13}C glucose in citrate and glutamate metabolites for free DOX-treated cells (**Figure 7, Panel D**), confirming the reduced glucose flux through glycolysis. On the other hand, citrate and glutamate enrichment was not altered by P1 and P2 conjugates compared to control cells upon adding U-^{13}C glucose. This suggests that P1/P2 achieved minimal inhibition on glucose utilization. Further, free DOX shifted the TCA cycle substrate utilization towards fatty acid oxidation instead of glucose oxidation, as expected. This is evident by the increased incorporation of ^{13}C carbons from oleate in citrate and glutamate metabolites (**Figure 7, Panel E**). In comparison, P1 increased fatty acid oxidation more than the control or P2 conjugates but less than free DOX (**Figure 7, Panel E**). While the reason for the differences in fatty acid oxidation caused by either P1 or P2 remains to be identified, it is evident that the metabolic response induced by the conjugates is significantly different from that caused by free DOX, particularly in terms of the effect on glucose and fatty acid oxidation.

These results suggest that G5-mediated delivery of DOX alters both its intracellular release and the associated cellular response. To the best of our knowledge, this is the first report establishing a relationship between the mode of delivery of a chemotherapeutic cargo using a polymeric carrier and the associated intracellular release, metabolism, and effect on metabolic pathways. We believe this warrants more attention and analysis of the intracellular fate of the therapeutic cargo delivered using different carriers (e.g. nanoparticles, antibodies) to establish a robust correlation between intracellular concentration-versus-time profiles. Such insight would allow accurate determination of

the anticipated therapeutic response *in vitro* and in preclinical animal models, which will facilitate clinical translation of these technologies.

3. Conclusion

We report the synthesis and *in vitro* validation of a nanoparticle-based drug delivery method aimed at improving the treatment of hepatocellular carcinoma. We synthesized NAcGal$_\beta$-targeted, DOX-loaded G5 PAMAM dendrimers (e.g. NAcGal$_\beta$-PEG*c*-G5-L(x)-DOX conjugates) in two different formulations based on our previous work, P1 or P2. We verified the biocompatibility of the two conjugates and showed that they achieved efficient internalization into hepatic cancer cells, which corresponded with controllable anticancer activity comparable to free DOX. We employed metabolomics to identify that P1 and P2 conjugates deliver DOX metabolites different than DOX delivered freely in solution, indicating differences in intracellular release of the drug based on the delivery method. Further, we established that the difference in delivered DOX metabolites also induced different metabolic responses within the treated cells. Despite alternate metabolomics profiles, our results indicate that P1 and P2 conjugates present viable nanoparticle-based delivery systems that can be used for controllable doxorubicin delivery to hepatic cancer tissue.

4. Experimental Section

Materials: G5-$(NH_2)_{128}$ dendrimers with a diaminobutane core were purchased from Andrews ChemServices (Berrien Springs, MI) and purified by dialysis against deionized water using Slide-A-Lyzer dialysis cassettes (MWCO 10 kDa, Thermo Fisher Scientific,

Rockford, IL) to remove imperfect dendrimers and debris. Doxorubicin-HCl was purchased from AvaChem Scientific (San Antonio, TX). *N*-acetylgalactosamine, 4-pentynoic acid, pyridine, trimethylphosphine solution (1.0 M in THF), triethylamine (TEA), acetic anhydride (Ac_2O), 1-ethyl-3-(3-dimethylaminopropyl) carbodiimide hydrochloric acid (EDC.HCl), benzotriazol-1-ol (HOBt), trifluoroacetic acid (TFA), bathophenonthroline sulfonated sodium salt (SBP), copper bromide (CuBr), anhydrous dimethylsulfoxide (DMSO), anhydrous dichloromethane (DCM), anhydrous dimethylformamide (DMF), anhydrous tetrahydrofuran (THF), *cis*-aconitic anhydride (cis-Ac), and bovine serum albumin (BSA) were purchased from Sigma-Aldrich Inc. (St. Louis, MO). Trimethylsilyl trifluoromethanesulfonate (TMSOTf), N,N-diisopropyl ethyl amine (DIPEA), camphor sulphonic acid (CSA), sodium azide (NaN_3), sodium ascorbate, and benzotriazol-1-yl-oxytripyrrolidinophosphonium hexafluorophosphate (PyBOP) were purchased from Across Organics Chemicals (Geel, Belgium). N-hydroxysuccinimide-poly(ethylene glycol)-Boc (2 kDa) was purchased from JenKem Technology USA Inc (Plano, TX). 2-{2-(2-Chloroethoxy)ethoxy}ethanol was purchased from TCI America (Portland, OR). Dialysis cassettes (MWCO 1–10 kDa) were purchased from Thermo Fisher Scientific (Rockford, IL). Minimum essential medium (MEM), OPTI-MEM reduced serum medium, fetal bovine serum (FBS), 0.25% trypsin/0.20% ethylenediaminetetraacetic acid (EDTA) solution, phosphate buffered saline (PBS), penicillin/streptomycin/amphotericin solution, sodium pyruvate, minimum non-essential amino acid (NEAA) solution, and 0.4% trypan blue solutions were purchased from Life Technologies (Thermo Fisher Scientific, Rockford, IL).

Spectra for Synthesis of Conjugates: Complete NMR and time-of-flight matrix-assisted laser desorption/ionization (MALDI-TOF) spectra confirming the structural identity and composition of NAcGal-*c*PEG-G5-L(x)-DOX (P1 and P2) conjugates can be found in the **Supporting Information**. Control particles were either purchased commercially (unmodified, cationic G5-$(NH_2)_{128}$ dendrimers) or synthesized according to our established protocols[18,76] (acetylated G5 (G5-$(Ac)_{128}$) and non-DOX-loaded ($NAcGal_\beta$-PEG*c*)$_{12.1}$-G5 conjugates (**P0**)).

*Synthesis of NAcGal-*c*PEG-G5-(NH_2)-alkyne:* We chose a similar approach to our previously published strategies in order to synthesize PEGylated, NAcGal-targeted G5 conjugates (**Figure 2**).[19,23] Briefly, D-galactosamine was treated with Ac_2 and Py to obtain D-galactopentaacetate (**1**), which was treated with TMSOT in DCM to obtain an oxazolidine derivative (compound **2**). The oxazolidine was reacted with an alcohol (compound **3**) in the presence of D-10-CSA in DMSO at 40 ^oC to yield compound **4**. The azide functional group of compound **4** was reduced to an amine with Me_3P and THF to obtain compound **5**, which facilitates coupling to the hetero bi-functional PEG with an NHS-activated COOH group. This peptide coupling was facilitated by EDC.HCl, HOBt, and DIPEA in DMF to obtain a PEG derivative (**6**) having $NAcGal_\beta$ at one end and on the other end a Boc-protected NH_2. The Boc group was deprotected by acid hydrolysis using TFA and DCM to unmask the terminal amine group (**7**), which was reacted with *cis*-aconitic anhydride to form the corresponding acid compound **8**. This acid was further treated with NaOMe in methanol to

deprotect the *O*-acetate groups from galactosamine to obtain acid **9**. We attached NAcGal-functionalized NAcGal$_\beta$-PEG chains (**9**) to G5 by reacting the *cis*-aconitic acid at the PEG end with alkyne-G5-NH_2 (**10**), which was synthesized via a peptide coupling reaction between G5-$(NH_2)_{128}$ dendrimers and 4-pentynoic acid in the presence of PyBOP and DIPEA in DMSO. The primary amine groups of G5 form peptide bonds with *cis*-aconityl acids in the presence of EDC.HCl and HOBt in 6.0 pH phosphate buffer solution to obtain conjugate **11** (**Figure 2**).

Click coupling of L(x)-DOX Conjugates: We synthesized NAcGal-cPEG-G5-L(x)-DOX conjugates by using a modified version of a standard click coupling procedure between conjugate **11** and L3/L4-DOX linkages following published protocols (**Figure 2**).[23] In brief, sodium ascorbate, bathophenonthroline sulfonate sodium salt (SBP), and Cu (I) were dissolved in 3 mL of a THF:water mixture (1:1) and bubbled with argon for 10 minutes to obtain an oxygen-free catalyst solution. This solution was heated to 75 °C for 3-4 minutes, resulting in a change in solution color to brick red, and then cooled to room temperature. In a separate flask, compound **11** (1 equivalent) and L3-DOX or L4-DOX (12 equivalents) were dissolved in a THF:water mixture (1:1) and bubbled with argon for 10 minutes. The catalyst solution was then added to this flask by a syringe under argon gas. The whole mixture was stirred slowly (~400 rpm) in the dark for 48 hours at room temperature. The reaction mixture was then purified by dialysis against deionized water (10kDa MWCO) for 2 days to obtain pure [(NAcGal$_\beta$-PEG*c*)$_{16.6}$-G5-(L3-DOX)$_{11.6}$] (P1) or [(NAcGal$_\beta$-PEG*c*)$_{16.6}$-G5-(L4-DOX)$_{13.4}$] (P2) conjugates dispersed in DI water (**Figure 2**). To obtain the concentration of

these conjugates, we lyophilized 1 mL of the particle solution and weighed the amount of dried conjugate remaining.

Characterization of P1 and P2 Conjugates: We measured the particle size of the nanoparticle formulations by dynamic light scattering (DLS) using a 90Plus particle size analyzer (Brookhaven Instruments, Holtsville, NY). The nanoparticle solution was diluted in DI water at 1:20 v/v with 10% tween 20 in order to limit nanoparticle aggregate formation. After sonication for 20 minutes, P1 and P2 conjugates were sterile-filtered through syringe filters with a pore size of 800 nm and warmed to 37 ℃ before measurements. Raw distribution data was plotted in Graphpad Prism software and fit using a Gaussian curve, with the mean being taken as the particle size for that replicate. The average of three separate replicates was taken to find the mean particle size ± standard error of the mean (SEM). We also determined the zeta potential of the conjugates using a 90Plus Zeta Potential Analyzer (Brookhaven Instruments, Holtsville, NY). Particle formulations were dissolved in DI water at 1:20 v/v and warmed to 37 ℃ before analysis. The average of three separate replicates was taken to find the mean zeta potential ± SEM.

Hemolysis Assay: We measured the extent of erythrocyte lysis caused by P1 and P2 conjugates using the RBCs hemolysis assay.[42,77] Briefly, we collected fresh blood from healthy human volunteers following IRB-approved protocols into EDTA-coated tubes and immediately centrifuged them at 3000 RPM for 5 minutes to precipitate out the red blood cells (RBCs). The supernatant was removed, and a 0.15 M NaCl wash solution was used to bring the RBCs up to the initial volume of blood. The

sample was spun again at 3000 RPM for 5 minutes, the supernatant removed, and the RBCs resuspended to the original volume. This cycle was repeated a third time before splitting the resuspended RBCs into three different EDTA-coated centrifuge tubes. These tubes were centrifuged at 3000 RPM for 5 minutes, and the level of the fluid was marked before removing the supernatant. PBS (1x, Gibco) was then added up to the original volume, and this solution was diluted 1:9 (v/v) in PBS to create the working stock solution. 200 µL of this working stock solution was added to each test tube, and treatment solutions of 1x PBS (negative control), DI water (positive control), 240 nM naked G5-$(NH_2)_{128}$ dendrimers, or 240 nM G5-equivalent of either P1 (2.78 µM DOX) or P2 (3.22 µM DOX) conjugates were added to the wells to achieve a final volume of 1mL. The samples were incubated for 1 hour at 37 °C and then mixed by inversion and centrifuged at maximum speed for 5 minutes. Finally, 200 µL of the supernatant was collected and added to 96-well plates, and the excitation of hemoglobin was measured by UV (λ_{ex}=541 nm). The raw data was normalized to PBS values (which is non-hemolytic due to its buffering capacity[35]) and presented as a percentage of hemolysis caused by DI water (which causes hemolysis through osmotic swelling and rupture of RBCs[35]). Results are presented as the mean of three replicates ± SEM.

Platelet Aggregation: We evaluated the interaction of platelets with P1 and P2 conjugates using light transmission platelet aggregometry according to published protocols.[42] Briefly, fresh blood was isolated from anesthetized C57BL/6 mice via cardiac puncture using 20 gauge needles flushed with 3.2% sodium citrate and was diluted 1:1 v/v with HEPES Tyrode (HT) buffer and centrifuged at 50xg for 10 minutes at room temperature. The supernatant was collected as platelet rich plasma (PRP), and the precipitate was resuspended in HT buffer up to the original volume and spun again at 50xg

for 10 minutes at room temperature. The supernatant was collected and added to the original PRP fraction, while the precipitate was resuspended with HT buffer to the original volume. After spinning the suspension at 1200xg for 10 minutes at room temperature, the supernatant was collected into a separate tube as the platelet poor plasma (PPP) fraction. We mixed either naked G5-$(NH_2)_{128}$ dendrimers, P0, P1, or P2 conjugates with 500 µL of PRP solution prewarmed to 37ºC to achieve a final G5-equivalent concentration of 240 nM. We monitored platelet aggregation over 10 minutes using the Aggro-Link data reduction system (Chrono-log Corporation, Havertown, PA). We also measured the platelet aggregation of 500 µL PRP incubated with PBS or 10 µM adenosine diphosphate (ADP) as negative or positive controls, respectively. Results are presented as the mean of three replicates ± SEM.

*Opsonization by Serum Proteins***:** We also assessed the extent of particle opsonization by measuring the binding of bovine serum albumin (BSA) as a model protein to P1 and P2 conjugates as a function of particle composition and time, based on our published protocols.[18] Briefly, we prepared G5-$(NH_2)_{128}$, $(NAcGal_{\beta}\text{-}PEG_c)_{12.1}$-G5 (**P0**), P1, and P2 conjugates in warmed PBS (pH 7.4) at a particle concentration of 241 nM. Conjugates were mixed with BSA (0.2 mg/mL) in a quartz cuvette and incubated at 37 °C for 60 minutes. The fluorescence of BSA tryptophan residues (λ_{ex}: 280 nm; λ_{em} scanned between 300-400 nm) was measured at time zero (I^0) and at different incubation times (I) up to 60 minutes in a QM4 fluorescence spectrophotometer (Perkin-Elmer, Waltham, MA). We divided the initial BSA fluorescence (I^0) by the measured fluorescence at different timepoints (I) to evaluate the extent of BSA quenching, as an indication of BSA binding to the particle's surface, indicated by $I^0/I > 1$. BSA adsorption to each particle was measured in triplicates and presented as

the mean $I^0/I \pm$ SEM. Statistical comparisons were made between the I^0/I values measured for conjugates and that observed with BSA alone using student's t-test.

Cell Culture: HepG2 and Hep3B cells were cultured in T-75 flasks using MEM supplemented with 10% FBS, 1% antibiotic-antimycotic, 1% sodium pyruvate, 1% non-essential amino acids, and 1 mL gentamicin. HepG2 and Hep3B cells were maintained at 37 ℃, 5% CO_2, and 95% relative humidity and medium was changed every 48 hours. The cells were passaged at 80-90% confluency using a 0.25% trypsin/0.20% EDTA solution.

Uptake of P1 and P2 conjugates into Hepatic Cancer cells: The internalization of P1 and P2 conjugates into HepG2 and Hep3B cells was measured as a function of particle composition and concentration via flow cytometry. Briefly, 250,000 HepG2 or Hep3B cells were seeded in 24-well plates and allowed to adhere overnight. Treatment solutions of P1 or P2 conjugates (7-285 nM G5 concentration; 100-4000 nM NAcGal concentration) were prepared in OPTI-MEM and then incubated with the cells for 2 hours at 37 ℃. We used free DOX treatments for comparison and included them at concentrations equivalent to the DOX loaded onto either P1 or P2 conjugates. We also used cells treated only with OPTI-MEM as a control. After removing the treatment medium and washing the cells with warmed PBS twice, the adherent cells were removed from the plates using a 0.25% trypsin/0.20% EDTA solution and then suspended in fresh culture medium. The cells were then transferred to flow cytometry tubes, centrifuged at 1000 RPM for 5 minutes at 4℃, kept on ice, and then resuspended immediately before analysis. Samples were analyzed by flow cytometry using the intrinsic fluorescence of

DOX (λ_{ex}: 488 nm; λ_{em}: 613 nm) on a Beckman Coulter Cyan ADP instrument provided by the Flow Cytometry Core at the University of Michigan (Ann Arbor, MI). Data is presented as the mean ± SEM for n=4 replicates, and we used untreated cells in blank OPTI-MEM as our negative control.

Cytotoxicity of P1 and P2 conjugates: The cytotoxicity of P1 and P2 conjugates against HepG2 and Hep3B cells was measured as a function of DOX concentration via the clonogenic survival assay.[23] Briefly, 250,000 HepG2 or Hep3B cells were plated in T-25 flasks and allowed to adhere overnight. Treatments of free DOX, P1, or P2 conjugates were prepared at equivalent DOX concentrations (1-10,000 nM DOX) in OPTI-MEM at a total volume of 5 mL and incubated with the cells for 72 hours. After the treatment period, the cells were washed twice with PBS, trypsinized with 0.25% trypsin/0.20% EDTA solution, collected into tubes, and centrifuged at 1000 RPM for 5 minutes. The supernatant was then aspirated and the cells were resuspended in 1 mL of fresh medium and kept on ice during counting. The cell count was established manually using a hemocytometer and were seeded into 6-well plates at either 1000 or 2000 cells per well in 3 mL of medium, with three replicates for each cell count. The cells were allowed to sit undisturbed for 14 days at 37 ℃ and 5% CO_2. The medium was then removed and the cells were washed with PBS once. The colonies were fixed and stained using 1 mL of a methanol/glacial acetic acid (75/25 v/v) solution with 0.04% w/v trypan blue and incubated for 15-30 minutes. The stain was then aspirated and the plates were allowed to dry uncovered for 20 minutes. The stained colonies

were counted by visual inspection. Plating efficiency (PE) was determined by dividing the number of control untreated colonies resulting from the known number seeded cells (1000 or 2000). The surviving fraction of treated cells was then determined by dividing the number of counted colonies by the PE. The surviving fraction across all six replicates was averaged and presented as % survival ± SEM.

Metabolomics analysis: To measure the intracellular release of either free DOX or P1/P2 conjugates as well as the associated metabolic response upon treatment, we applied metabolomics analysis on treated cells, as described previously.[78–80] For treatment, $1x10^6$ HepG2 cells were seeded in 6-well plates and allowed to adhere and double in population over 24 hours. Treatment solutions of free DOX (10 μM) or P1 and P2 (10 μM DOX-equivalent) in OPTI-MEM were incubated with the cells for 12 hours. After treatment, cell plates were rinsed with 200 mM ammonium acetate and quenched with liquid nitrogen. Metabolites were extracted with ice cold 8:1:1 methanol:chloroform:water and assayed by high performance liquid chromatography coupled to time-of-flight mass spectrometry (HPLC-TOF-MS). For polar metabolites, chromatographic separation was performed using an Agilent Technologies (Santa Clara, CA) 1200 HPLC system equipped with a Phenomenex (Torrance, CA) Luna NH_2 HPLC column (1.0 mm inner bore × 150 mm long and packed with 3 μm particles). Mobile phase A was 100% acetonitrile (ACN) and mobile phase B (MPB) was 100% 5 mM ammonium acetate adjusted to pH 9.9 with ammonium hydroxide. The gradient started at 20% MPB and was ramped to 100 % MPB over 20 minutes, held for 5

minutes, and returned to 20% MPB for an additional 7 minutes. Doxorubicin and its metabolites were separated using an Acquity UPLC® BEH C18 column (2.1 × 100 mm, 1.7 μm) and a 2.1 × 5 mm VanGuard™ pre-column using the following conditions: mobile phase A of 0.1 % formic acid and mobile phase B of acetonitrile with 0.1% formic acid. The gradient was started at 5% B and progressed to 100% B in 25 minutes followed by being held at 100% B for 10 minutes before reconditioning the column back to 5% B for 10 more minutes.

For isotope tracer studies, after the same treatment for 12 hours by either free DOX, P1, or P2, the treatment media was replaced by media containing a stable isotope tracer. One medium contained 10 mM U-^{13}C glucose and 100 μM oleate while the other contained 10 mM glucose and 100 μM U-^{13}C oleate. Cells were incubated for 4 hours before being quenched and analyzed for metabolites as described above.

Data analysis and statistics: Targeted analysis was performed to measure specific metabolites involved in central carbon metabolism such as glycolysis and TCA cycle intermediates. Untargeted analysis was performed using XCMS online.[81] Features that showed substantial differences were manually quantified and their masses were checked against both Human Metabolome Database (HMDB) and METLIN.

Supporting Information

Supporting Information is available from the Wiley Online Library or from the author.

Acknowledgements

The authors would like to thank Dr. Jinsang Kim and Dr. Daniel Eitzman for providing access to their fluorescence spectrophotometer and light aggregometry instrument, respectively, as well as the Michigan Regional Comprehensive Metabolomics Resource Core (MRC2) for support with the metabolomics work (NIH Grant #U24DK097153). Sibu P. Kuruvilla recognizes the support of the NSF Graduate Research Fellowship (GRFP) award and the University of Michigan Rackham Merit Fellowship (RMF). Sibu P. Kuruvilla and Gopinath Tiruchinapally contributed equally to this research work.

Received: ((will be filled in by the editorial staff))
Revised: ((will be filled in by the editorial staff))
Published online: ((will be filled in by the editorial staff))

[1] A. G. Singal, J. A. Marrero, *Curr. Opin. Gastroenterol.* **2010**, *26*, 189.

[2] J. Ferlay, I. Soerjomataram, M. Ervik, R. Dikshit, S. Eser, C. Mathers, M. Rebelo, D. M. Parkin, D. Forman, F. Bray, GLOBOCAN 2012 v1.0, Cancer Incidence and Mortality Worldwide: IARC CancerBase. No. 11 [Internet]. *Lyon, Fr. Int. Agency Res. Cancer.* **2013**, *11*, http://globocan.iarc.f.

[3] A. G. Singal, H. B. El-Serag, *Clin. Gastroenterol. Hepatol.* **2015**, *13*, 2140.

[4] H. B. El-Serag, *Hepatol. Res.* **2007**, *37*, S88.

[5] J. L. Petrick, S. P. Kelly, S. F. Altekruse, K. A. McGlynn, P. S. Rosenberg, *J. Clin. Oncol.* **2016**, *34*,

1787.

[6] D. Miyaki, H. Aikata, Y. Honda, N. Naeshiro, T. Nakahara, M. Tanaka, Y. Nagaoki, T. Kawaoka, S. Takaki, K. Waki, A. Hiramatsu, S. Takahashi, M. Ishikawa, H. Kakizawa, K. Awai, K. Chayama, *J. Gastroenterol. Hepatol.* **2012**, *27*, 1850.

[7] S. W. Shin, *Korean J Radiol* **2009**, *10*, 425.

[8] R. Yamada, K. Kishi, M. Sato, T. Sonomura, N. Nishida, K. Tanaka, Y. Shioyama, M. Terada, M. Kimura, *World J. Surg.* **1995**, *19*, 795.

[9] T. J. Vogl, N. N. N. Naguib, N.-E. A. Nour-Eldin, P. Rao, A. H. Emami, S. Zangos, M. Nabil, A. Abdelkader, *Eur. J. Radiol.* **2009**, *72*, 505.

[10] E. Garwood, N. Fidelman, S. Hoch, R. Kerlan Jr, F. Yao, *Liver Transplant.* **2013**, *19*, 164.

[11] I. Idilman, B. Peynircioglu, B. E. Cil, B. Doganay Erdogan, S. Yalcin, Y. Bayraktar, T. Kav, K. Altundag, F. Balkanci, *Turkish J. Gastroenterol.* **2013**, *24*, 141.

[12] H.-Y. Cheng, X. Wang, D. Chen, A.-M. Xu, Y.-C. Jia, *World J. Gastroenterol.* **2005**, *11*, 3644.

[13] K. Barnett, M. Malafa, *Int. J. Gastrointest. Cancer* **2001**, *30*, 147.

[14] A. Basile, G. Carrafiello, A. M. Ierardi, D. Tsetis, E. Brountzos, *Cardiovasc. Intervent. Radiol.* **2012**, *35*, 765.

[15] O. Fardel, E. Jigorel, M. Le Vee, L. Payen, *Biomed. Pharmacother.* **2005**, *59*, 104.

[16] V. Gajbhiye, V. K. Palanirajan, R. K. Tekade, N. K. Jain, *J. Pharm. Pharmacol.* **2009**, *61*, 989.

[17] H. Liu, H. Wang, Y. Xu, R. Guo, S. Wen, Y. Huang, W. Liu, M. Shen, J. Zhao, G. Zhang, X. Shi, *ACS Appl. Mater. Interfaces* **2014**, *6*, 6944.

[18] S. H. Medina, G. Tiruchinapally, M. V. Chevliakov, Y. Y. Durmaz, R. N. Stender, W. D. Ensminger, D. S. Shewach, M. E. H. ElSayed, *Adv. Healthc. Mater.* **2013**, *2*, 1337.

[19] S. H. Medina, V. Tekumalla, M. V Chevliakov, D. S. Shewach, W. D. Ensminger, M. E. H. El-Sayed, *Biomaterials* **2011**, *32*, 4118.

[20] H. Mu, K.-X. Lin, H. Zhao, S. Xing, C. Li, F. Liu, H.-Z. Lu, Z. Zhang, Y.-L. Sun, X.-Y. Yan, J.-Q. Cai, X.-H. Zhao, *World J. Gastroenterol.* **2014**, *20*, 5826.

[21] Y. Cao, Y. He, H. Liu, Y. Luo, M. Shen, J. Xia, X. Shi, *J. Mater. Chem. B* **2015**, *3*, 286.

[22] D. Ouyang, H. Zhang, H. S. Parekh, S. C. Smith, *Biophys. Chem.* **2011**, *158*, 126.

[23] S. H. Medina, M. V Chevliakov, G. Tiruchinapally, Y. Y. Durmaz, S. P. Kuruvilla, M. E. H. Elsayed, *Biomaterials* **2013**, *34*, 4655.

[24] A. R. Nicholas, M. J. Scott, N. I. Kennedy, M. N. Jones, *Biochim. Biophys. Acta* **2000**, *1463*.

[25] S. Kaufman, O. Borisov, M. Textor, E. Reimhult, *Soft Matter* **2011**, *7*, 9267.

[26] S. Honary, F. Zahir, *Trop. J. Pharm. Res.* **2013**, *12*, 265.

[27] M. Longmire, P. L. Choyke, H. Kobayashi, *Nanomedicine* **2008**, *3*, 703.

[28] H. S. Choi, W. Liu, P. Misra, E. Tanaka, J. P. Zimmer, B. Itty, M. G. Bawendi, J. V Frangioni, *Nat. Biotechnol.* **2009**, *25*, 1165.

[29] N. Bertrand, J. Wu, X. Xu, N. Kamaly, O. C. Farokhzad, *Adv. Drug Deliv. Rev.* **2014**, *66*, 2.

[30] J. Fang, H. Nakamura, H. Maeda, *Adv. Drug Deliv. Rev.* **2011**, *63*, 136.

[31] H. Maeda, G. Y. Bharate, J. Daruwalla, *Eur. J. Pharm. Biopharm.* **2009**, *71*, 409.

[32] R. Duncan, Y.-N. Sat-Klopsch, A. M. Burger, M. C. Bibby, H. H. Fiebig, E. a Sausville, *Cancer Chemother. Pharmacol.* **2013**, *72*, 417.

[33] J. B. Pryor, B. J. Harper, S. L. Harper, *Int. J. Nanomedicine* **2014**, *9*, 1947.

[34] S. Sadekar, H. Ghandehari, *Adv. Drug Deliv. Rev.* **2012**, *64*, 571.

[35] W. Xue, Y. Feng, F. Wang, Y. Guo, P. Li, L. Wang, Y. Liu, *Nat. Publ. Gr.* **2016**, 1.

[36] B. Klajnert, S. Pikala, M. Bryszewska, *Proc. R. Soc. A Math. Phys. Eng. Sci.* **2009**, *466*, 1527.

[37] H.-T. Chen, M. F. Neerman, A. R. Parrish, E. E. Simanek, *J. Am. Chem. Soc.* **2004**, *162*, 10044.

[38] V. Gajbhiye, P. V. Kumar, R. K. Tekade, N. K. Jain, *Curr. Pharm. Des.* **2007**, *13*, 415.

[39] W. Wang, W. Xiong, Y. Zhu, H. Xu, X. Yang, *J. Biomed. Mater. Res. - Part B Appl. Biomater.* **2010**, *93*, 59.

[40] V. Gajbhiye, P. Vijayaraj Kumar, R. K. Tekade, N. K. Jain, *Eur. J. Med. Chem.* **2009**, *44*, 1155.

[41] K. Xiao, Y. Li, J. Luo, J. S. Lee, W. Xiao, A. M. Gonik, R. G. Agarwal, K. S. Lam, *Biomaterials* **2011**, *32*, 3435.

[42] O. Aydin, I. Youssef, Y. Y. Durmaz, G. Tiruchinapally, M. E. H. Elsayed, **2016**.

[43] D. Woulfe, J. Yang, L. Brass, *J. Clin. Invest.* **2001**, *107*, 1503.

[44] A. Radomski, P. Jurasz, D. Alonso-Escolano, M. Drews, M. Morandi, T. Malinski, M. W. Radomski, *Br. J. Pharmacol.* **2005**, *146*, 882.

[45] D. E. Owens, N. a Peppas, D. E. Owens III, N. a Peppas, *Int. J. Pharm.* **2006**, *307*, 93.

[46] S. M. Moghimi, J. Szebeni, *Prog. Lipid Res.* **2003**, *42*, 463.

[47] F. Fu, Y. Wu, J. Zhu, S. Wen, M. Shen, X. Shi, *ACS Appl. Mater. Interfaces* **2014**, *6*, 16416.

[48] O. Khorev, D. Stokmaier, O. Schwardt, B. Cutting, B. Ernst, *Bioorg. Med. Chem.* **2008**, *16*, 5216.

[49] B. Thapa, P. Kumar, H. Zeng, R. Narain, *Biomacromolecules* **2015**, *16*, 3008.

[50] C. H. Wu, G. Y. Wu, **1998**, 1304.

[51] A. Shiber, W. Breuer, T. Ravid, *Prion* **2014**, *8*, 276.

[52] L. Y. Chan, B. A. Sc, E. K. F. Yim, D. Ph, A. B. H. Choo, **2012**, *0*, 1.

[53] A. L. Schwartz, S. E. Fridovich, B. B. Knowles, H. F. Lodish, *J. Biol. Chem.* **1981**, *256*, 8878.

[54] Y. Li, G. Huang, J. Diakur, L. I. Wiebe, *Curr. Drug Deliv.* **2008**, *5*, 299.

[55] T. K.-W. Lee, T. C.-M. Lau, I. O.-L. Ng, *Cancer Chemother. Pharmacol.* **2002**, *49*, 78.

[56] H. S. Yoo, K. H. Lee, J. E. Oh, T. G. Park, *J. Control. Release* **2000**, *68*, 419.

[57] R. Liu, D. Li, B. He, X. Xu, M. Sheng, Y. Lai, G. Wang, Z. Gu, *J. Control. Release* **2011**, *152*, 49.

[58] F. Capone, E. Guerriero, A. Sorice, G. Colonna, G. Storti, J. Pagliuca, G. Castello, S. Costantini, *ScientificWorldJournal.* **2014**, *2014*, 450390.

[59] R. D. Arnold, J. E. Slack, R. M. Straubinger, *J. Chromatogr. B* **2004**, *808*, 141.

[60] E. L. Westman, M. J. Canova, I. J. Radhi, K. Koteva, I. Kireeva, N. Waglechner, G. D. Wright, *Chem. Biol.* **2012**, *19*, 1255.

[61] D. Kaushik, G. Bansal, *J. Pharm. Anal.* **2015**, *5*, 285.

[62] M. Mondon, B. Renoux, P. Martin, B. Pfeiffer, P. Renard, A. Pierre, **2002**, *10*, 253.

[63] M. Gan, B. Liu, Y. Tan, Q. Wang, H. Zhou, H. He, Y. Ping, Z. Yang, Y. Wang, C. Xiao, *J. Nat. Prod.* **2015**, *78*, 2260.

[64] P. G. Guilfoile, C. R. Hutchinson, *J. Bacteriol.* **1992**, *174*, 3651.

[65] M. J. H. Janssen, D. J. A. Crommelin, G. Storm, A. Hulshoff, *Int. J. Pharm.* **1985**, *23*, 1.

[66] F. Greco, M. J. Vicent, S. Gee, A. T. Jones, J. Gee, R. I. Nicholson, R. Duncan, *J. Control. Release* **2007**, *117*, 28.

[67] B. Cao, M. Li, W. Zha, Q. Zhao, R. Gu, **2013**, 960.

[68] K. Kim, J. Yang, S. Jun, H. Sik, D. Hyun, Y. Kim, J. Yun, D. Soo, S. Min, **2013**, 1251.

[69] M. N. Triba, A. Starzec, N. Bouchemal, E. Guenin, G. Y. Perret, L. Le Moyec, *NMR Biomed.* **2010**, *23*, 1009.

[70] K. Wu, I. Kryczek, L. Chen, W. Zou, T. H. Welling, *Cancer Res.* **2009**, *69*, 8067.

[71] Y. Song, R. Zhao, Y. Hu, F. Hao, N. Li, G. Nie, H. Tang, Y. Wang, *J. Proteome Res.* **2015**, *14*, 5193.

[72] S. B. Wu, Y. H. Wei, *Biochim. Biophys. Acta - Mol. Basis Dis.* **2012**, *1822*, 233.

[73] G. N. Valbuena, M. Rizzardini, S. Cimini, A. P. Siskos, C. Bendotti, L. Cantoni, H. C. Keun, *Mol Neurobiol* **2015**, 2222.

[74] T. Jayasena, A. Poljak, N. Braidy, G. Smythe, M. Raftery, M. Hill, H. Brodaty, J. Trollor, N. Kochan, P. Sachdev, *PLoS One* **2015**, *10*, 1.

[75] Q. Niu, Z. Li, G. Du, X. Qin, *J. Pharm. Biomed. Anal.* **2016**, *118*, 338.

[76] S. H. Medina, M. E. H. El-Sayed, *Chem. Rev.* **2009**, *109*, 3141.

[77] Y. L. Lin, G. Jiang, L. K. Birrell, M. E. H. El-Sayed, *Biomaterials* **2010**, *31*, 7150.

[78] M. El-Azzouny, C. R. Evans, M. K. Treutelaar, R. T. Kennedy, C. F. Burant, *J. Biol. Chem.* **2014**, *289*, 13575.

[79] M. A. Lorenz, M. A. El Azzouny, R. T. Kennedy, C. F. Burant, *J. Biol. Chem.* **2013**, *288*, 10923.

[80] M. A. ElAzzouny, C. R. Evans, C. F. Burant, R. T. Kennedy, *PLoS One* **2015**, *10*, 1.

[81] R. Tautenhahn, G. J. Patti, D. Rinehart, G. Siuzdak, *Anal. Chem.* **2012**, *84*, 5035.

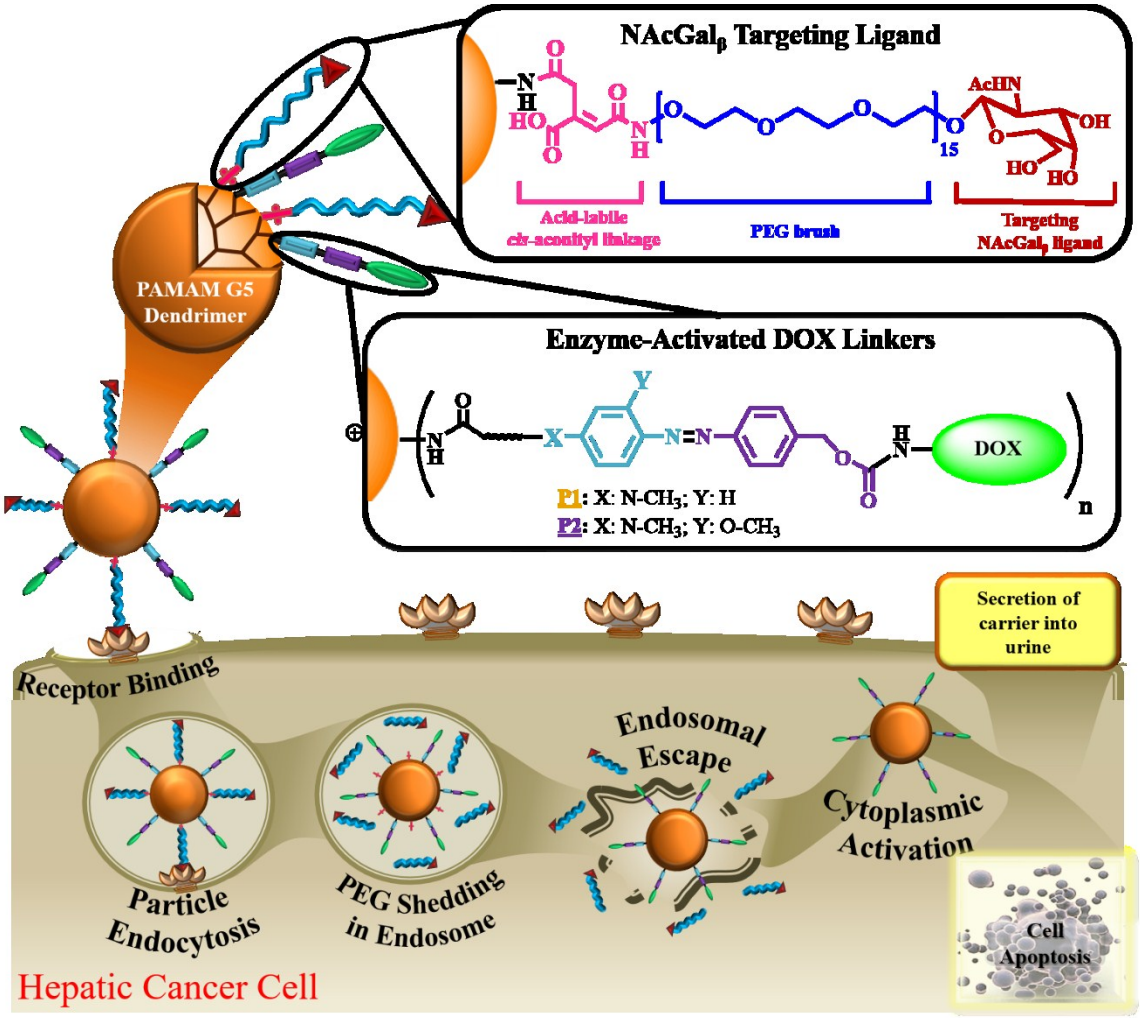

Figure 1. Strategy for targeted, enzyme-activated delivery of doxorubicin to hepatic cancer cells. We functionalized G5 PAMAM dendrimers with N-acetylgalactosamine (NAcGal)$_\beta$-terminated PEG brushes attached to G5 via an acid-labile cis-aconitic (*c*) spacer to facilitate selective binding to the asialoglycoprotein receptor (ASGPR) overexpressed on hepatic cancer cells. We also attached doxorubicin (DOX) molecules via two different enzyme-sensitive linkages to form either (NAcGal$_\beta$-PEG*c*)$_{16.6}$-G5-(L3-DOX)$_{11.6}$ (**P1**) or (NAcGal$_\beta$-PEG*c*)$_{16.6}$-G5-(L4-DOX)$_{13.4}$ (**P2**) conjugates. After internalization into the cancer cell via receptor-mediated endocytosis, P1/P2 conjugates shed the NAcGal$_\beta$-PEGc branches in the acidic endosome and undergo endosomal escape via the proton sponge effect. In the cytoplasm, the DOX linkages are selectively cleaved by hepatic azoreductase enzymes and release either DOX or DOX-related metabolites that are able to induce tumor cell apoptosis, while the carrier is excreted into the urine.

Particle Name	Chemical Composition	MW (Da)	Particle Size (nm)	Zeta Potential (mV)
G5-(Ac)$_{128}$	G5-(Ac)$_{128}$	34,200	5.59 ± 0.56	1.22 ± 1.44
P0	(NAcGal$_{\beta}$-PEG*c*)$_{12.1}$-G5	59,171	7.43 ± 0.34	-0.30 ± 0.21
P1	(NAcGal$_{\beta}$-PEG*c*)$_{16.6}$-G5-(L3-DOX)$_{11.6}$	84,572	6.02 ± 0.28	-0.63 ± 0.28
P2	(NAcGal$_{\beta}$-PEG*c*)$_{16.6}$-G5-(L4-DOX)$_{13.4}$	85,533	6.39 ± 0.40	-0.46 ± 0.23

Table 1. Physicochemical properties of G5-based conjugates

i) Synthesis of (2R,3R,4R,5R,6R)-5-acetamido-2-(acetoxymethyl)-6-(2-(2-(2-aminoethoxy)-ethoxy)-ethoxy)tetrahydro-2H-pyran-3,4-diyl diacetate (5)

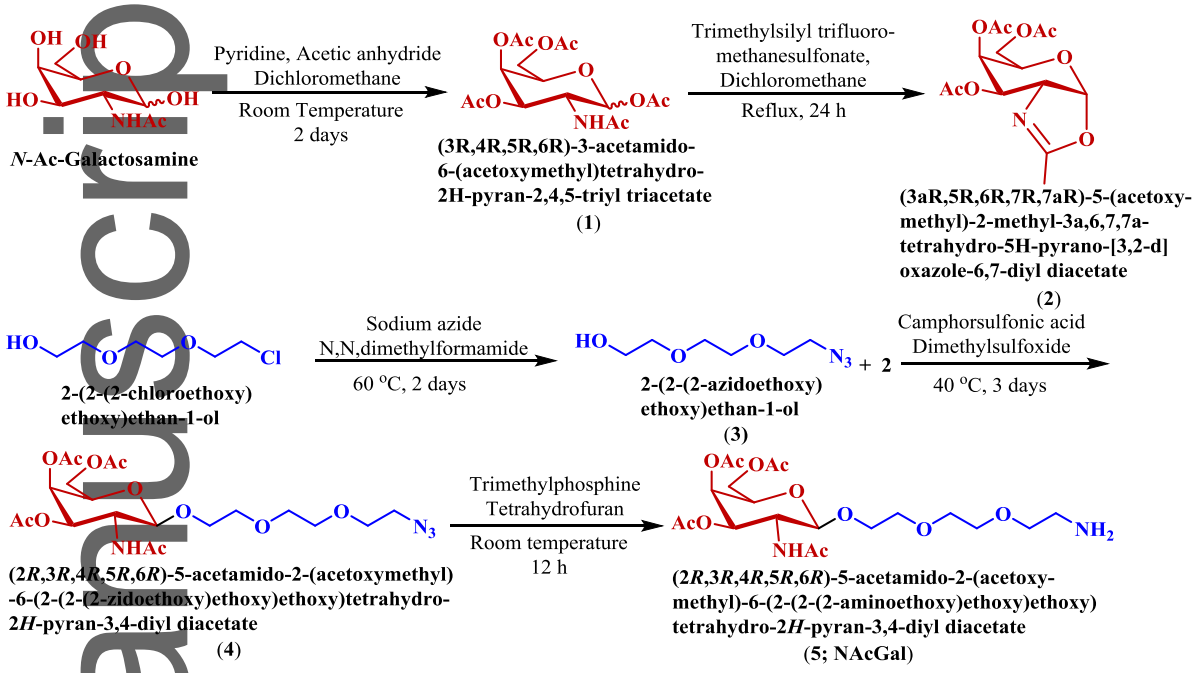

ii) Synthesis of NAc-Gal-PEG-CisAc (9)

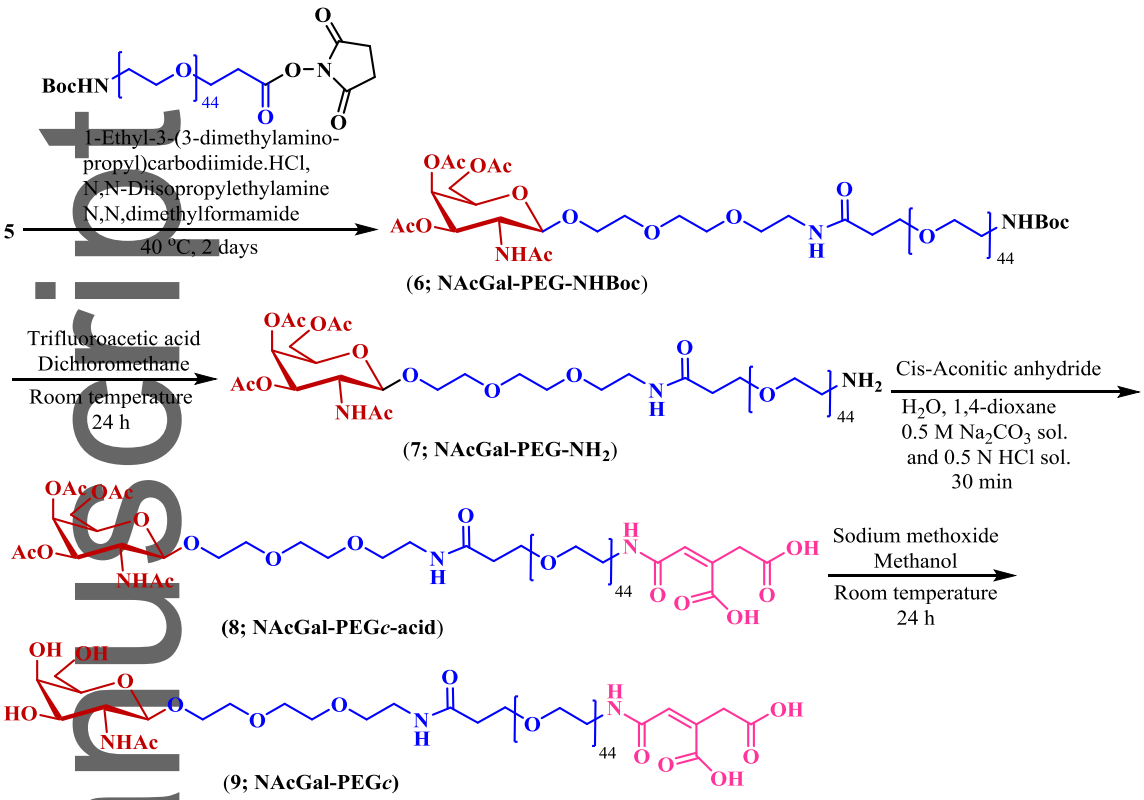

iii) Synthesis of G5-alkyne and its coupling to NAcGal-PEG-CisAc

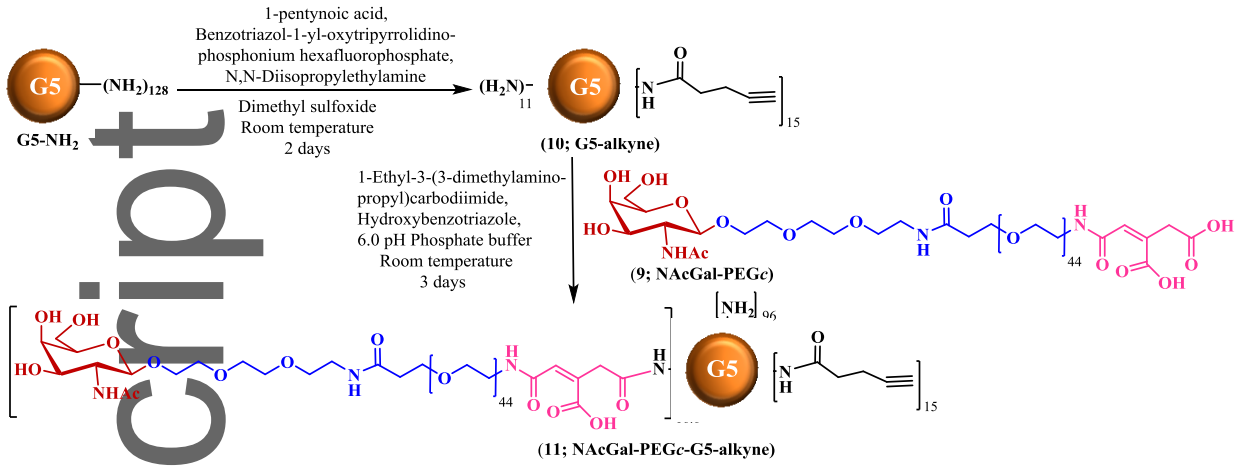

iv) Coupling of L3-DOX and L4-DOX to NAcGal$_\beta$-PEGc-G5-alkyne to form P1/P2 conjugates

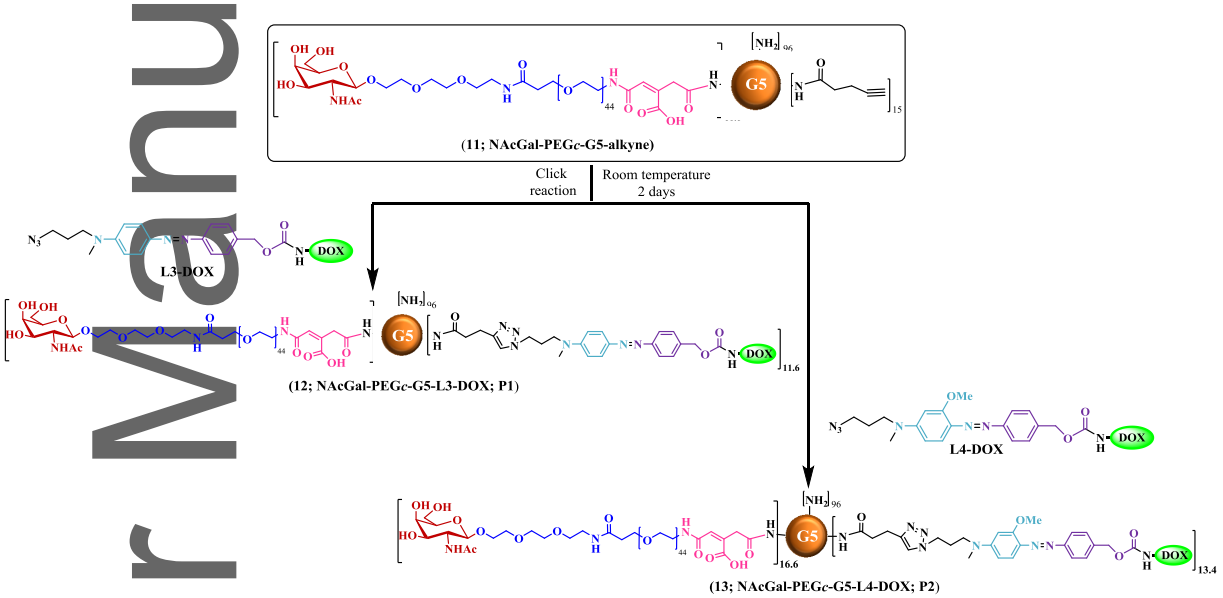

Figure 2. Synthesis of P1 and P2 conjugates. To achieve NAcGal$_\beta$-targeted, DOX-loaded nano-conjugates we first functionalized the G5 surface with 16.6 moles of NAcGal$_\beta$-targeted PEG brushes attached via an acid-labile cis-aconitic linkage. We then loaded either 11.6 moles of L3-DOX molecules or 13.4 moles of L4-DOX molecules via click-coupling to achieve P1 and P2, respectively. P1 and P2 particles have hydrodynamic diameters of 6.02 and 6.39 nm, respectively, and molecular weights of 84,572 or 85,533 Da.

(A)

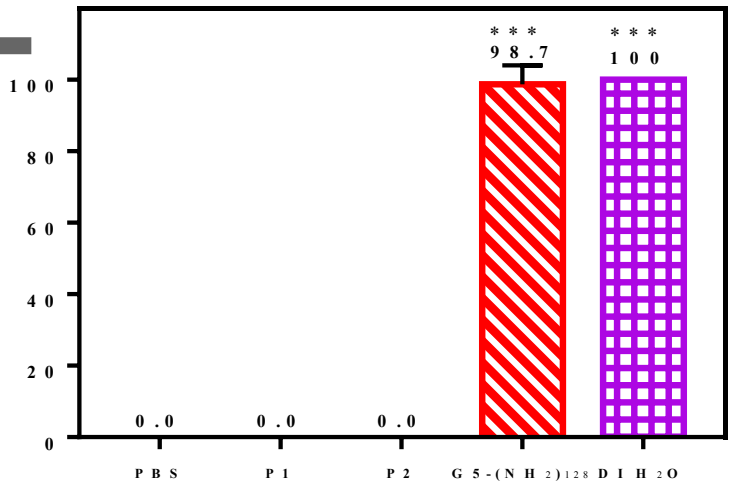

(B)

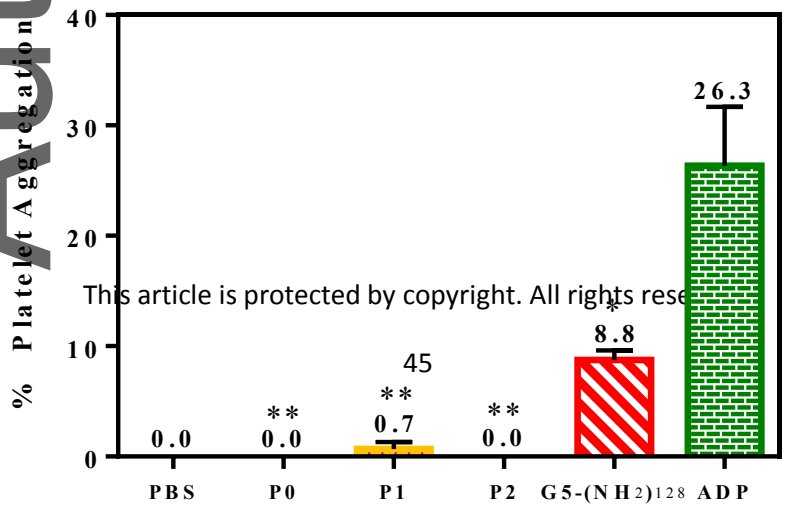

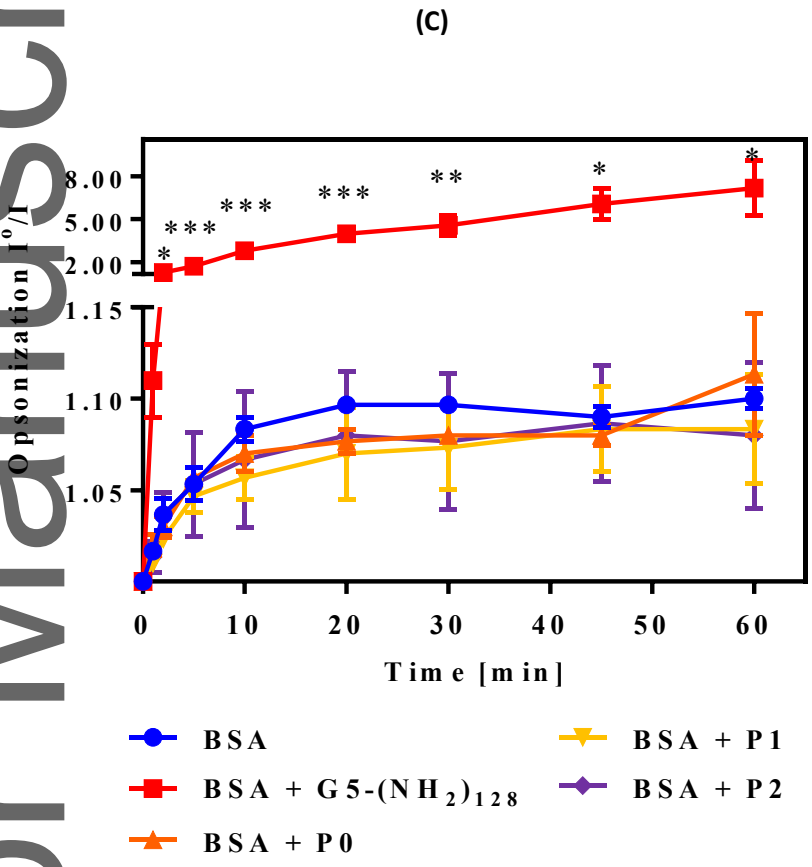

Figure 3. Biocompatibility of P1 and P2 conjugates. We evaluated the biocompatibility of P1 and P2 conjugates by measuring the extent of hemolysis **(A)**, platelet aggregation **(B)**, and opsonization by serum proteins **(C)**. Results show that P1 and P2 induce no hemolysis in red blood cells compared to PBS controls **(A)**, and they also do not cause aggregation of platelets **(B)**. Further, opsonization studies show that P1 and P2 are able to escape recognition by

serum proteins due to their neutral charge and PEG corona **(C)**. Results are presented as the means of at least three replicates ± SEM. Two-tailed Student's t-tests were used to determine the statistical difference between each treatment and the positive control of the respective study (DI H_20, ADP, or G5-$(NH_2)_{128}$, respectively), which is denoted by * for $p<0.05$, ** for $p<0.01$, and *** for $p<0.001$.

(A)

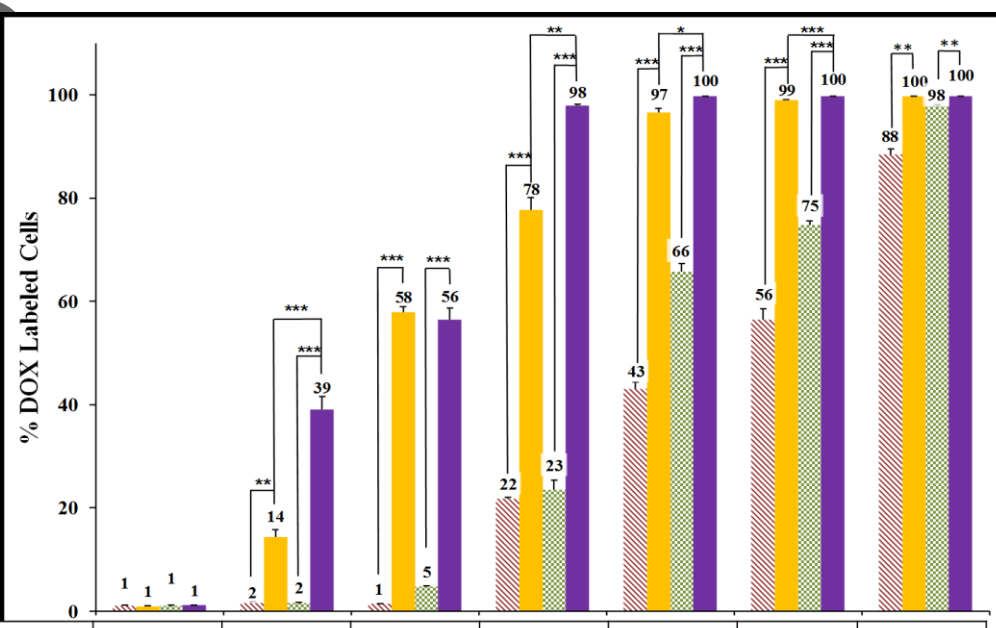

DOX Concentration (nM)	for P1	7.0	70	175	349	699	1398	2795
	for P2	8.1	81	202	404	807	1615	3229
Particle Concentration (nM)		0.6	6	15	30	60	120	240
NAcGal Concentration (nM)		10	100	250	500	1000	2000	4000

(B)

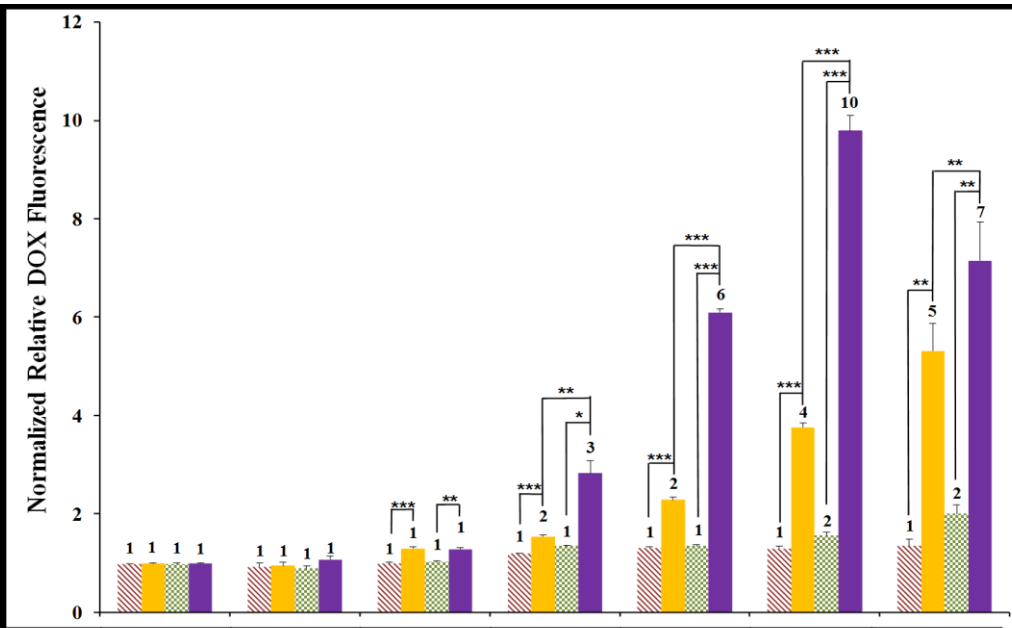

DOX Concentration (nM)	for P1	7.0	70	175	349	699	1398	2795
	for P2	8.1	81	202	404	807	1615	3229
Particle Concentration (nM)		0.6	6	15	30	60	120	240
NAcGal Concentration (nM)		10	100	250	500	1000	2000	4000

(C)

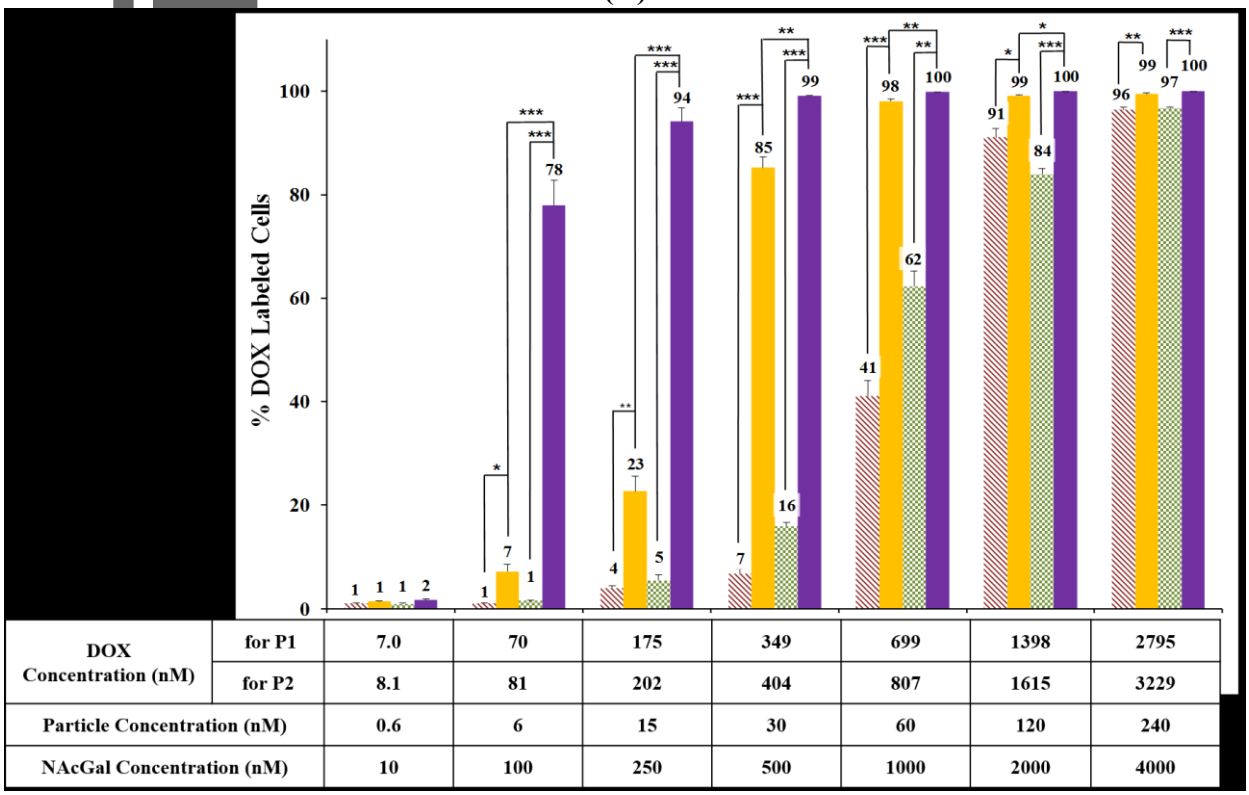

DOX Concentration (nM)	for P1	7.0	70	175	349	699	1398	2795
	for P2	8.1	81	202	404	807	1615	3229
Particle Concentration (nM)		0.6	6	15	30	60	120	240
NAcGal Concentration (nM)		10	100	250	500	1000	2000	4000

(D)

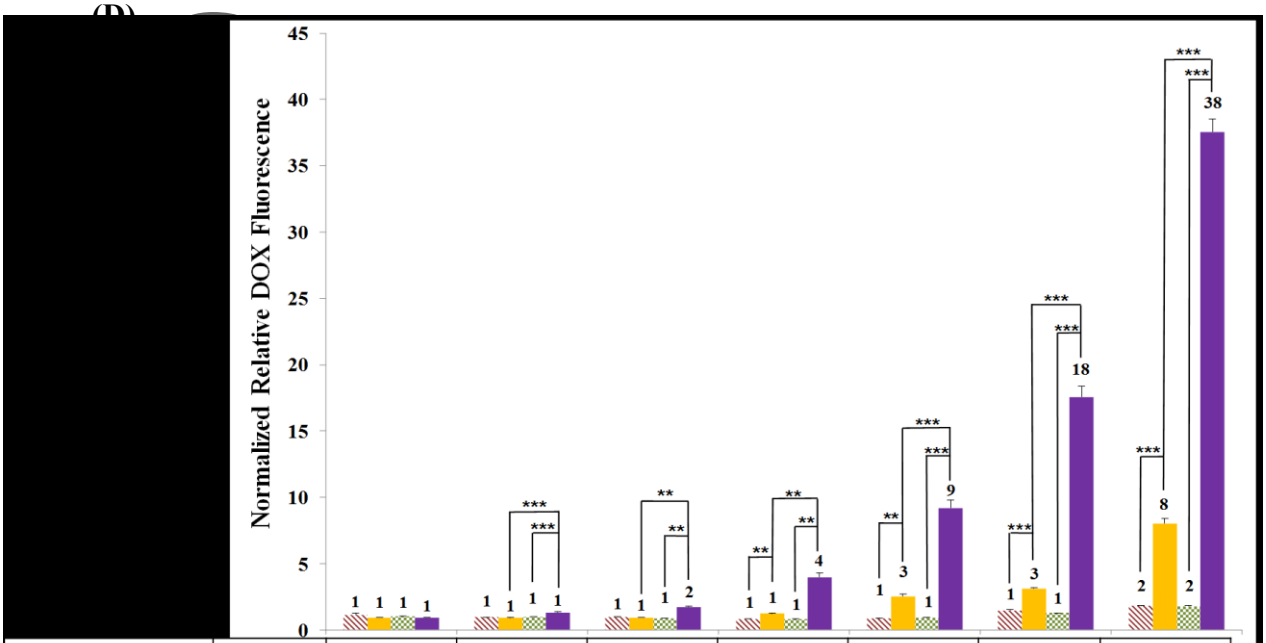

DOX Concentration (nM)	for P1	7.0	70	175	349	699	1398	2795
	for P2	8.1	81	202	404	807	1615	3229
Particle Concentration (nM)		0.6	6	15	30	60	120	240
NAcGal Concentration (nM)		10	100	250	500	1000	2000	4000

Figure 4. Uptake of P1 and P2 conjugates into HepG2 and Hep3B cells. We measured the internalization of P1 and P2 conjugates into hepatic cancer cells in comparison to free DOX via flow cytometry. P1 and P2 were incubated at NAcGal concentrations of 10-4,000 nM for 2 hours at 37ºC, and their equivalent DOX-loaded concentrations were used for free DOX

incubations, as shown in the table. Results show that both P1 and P2 label a significantly higher number of cells than their free DOX counterparts **(A, C)**, and this leads to as high as a 38-fold increase in intracellular fluorescence **(B, D)**. Results are presented as the means of three replicates ± SEM. Two-tailed Student's t-tests were used to determine the statistical difference between each treatment and is denoted by * for $P<0.05$, ** for $P<0.01$, and *** for $P<0.001$.

(A)

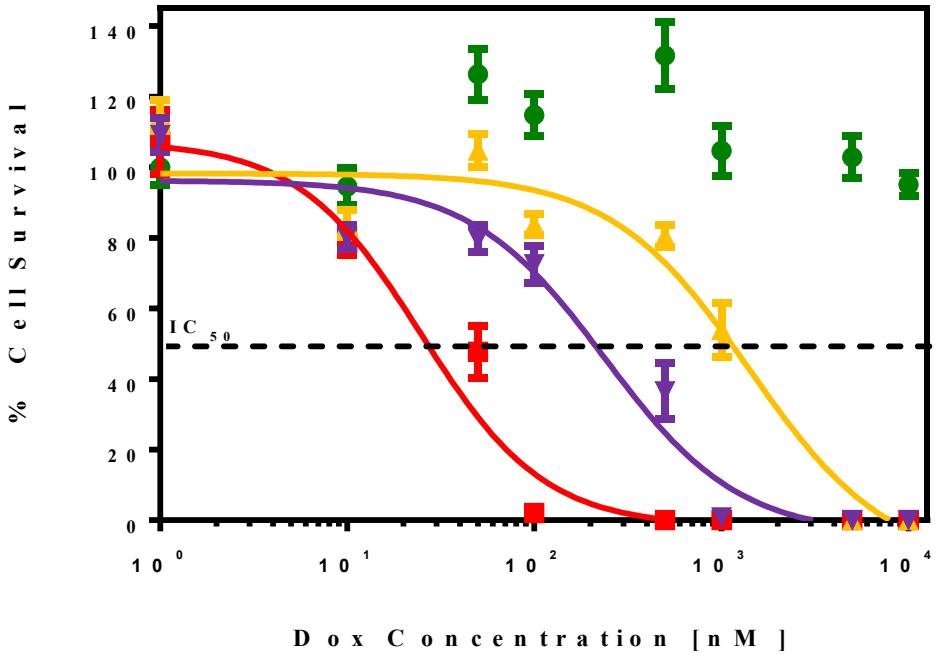

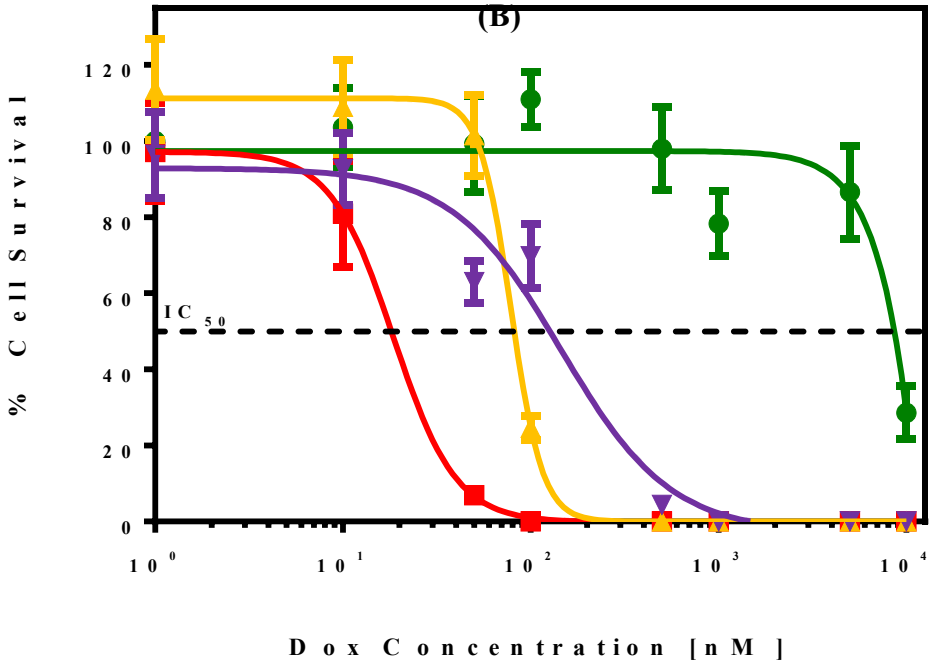

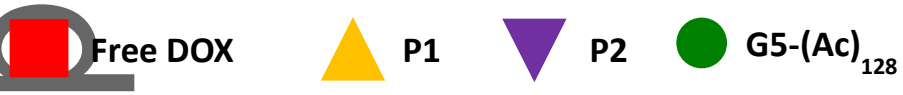

Figure 5. Anticancer activity of P1 and P2 conjugates against HepG2 and Hep3B cells. We measured the cytotoxicity profiles of P1 and P2 compared to free DOX against hepatic cancer cells after a 72-hour treatment via the clonogenic survival assay. Results show that in HepG2 cells **(A)**, free DOX, P1, and P2 exhibit IC_{50} values of 24.8 ± 1.19, 1414.0 ± 1.42, and 237.8 ± 1.20 nM, respectively. In Hep3B cells **(B)**, IC_{50} values were 18.6 ± 1.26, 78.5 ± 1.1, 145.5 ± 1.3 nM, respectively. The non DOX-loaded P0 carrier showed no (≥10,000 nM) toxicity in either cell line. Results are presented as the means of three replicates ± SEM.

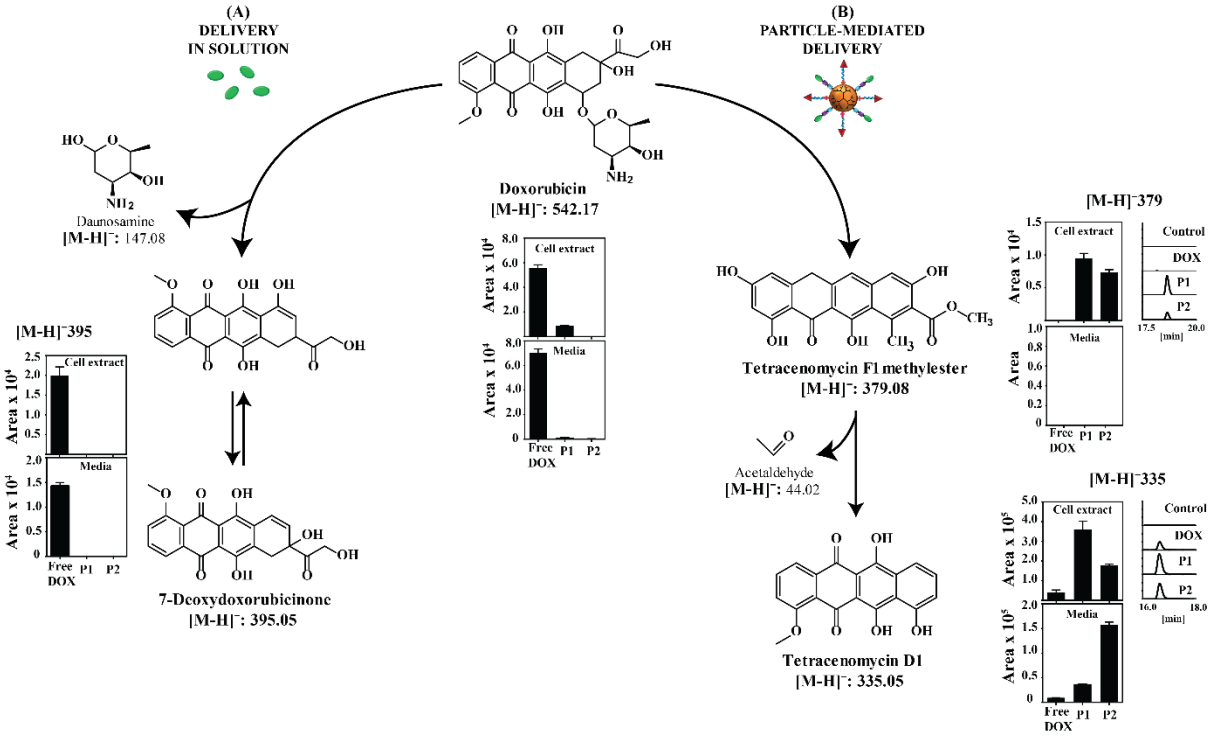

Figure 6. Metabolomics identifies different DOX-related metabolites delivered by P1 and P2 conjugates. We employed metabolomics to determine the chemical fingerprints of DOX delivered by P1 and P2 conjugates in comparison to DOX delivered freely in solution after a 12 hour treatment of HepG2 cells. Results show that free DOX generates two different metabolites: parent DOX ([M-H]⁻: 542.1710) and its deglycosylated form, 7-deoxydoxorubicinone ([M-H]⁻: 395.0587) **(A)**. P1 and P2 conjugates deliver other DOX-related metabolites, namely tetracenomycin analogues F1 methylester ([M-H]⁻: 379.0823) and D1 ([M-H]⁻: 335.0561) **(B)**. Intracellular and extracellular abundance of each metabolite is presented as the mean of three replicates ± SEM. Two-tailed Student's t-tests were used to determine the statistical difference between P1 or P2 compared to free DOX (*) or between P1 and P2 (#), and are denoted by * or # for P<0.05, ** or ## for P<0.01, and *** or ### for P<0.001.

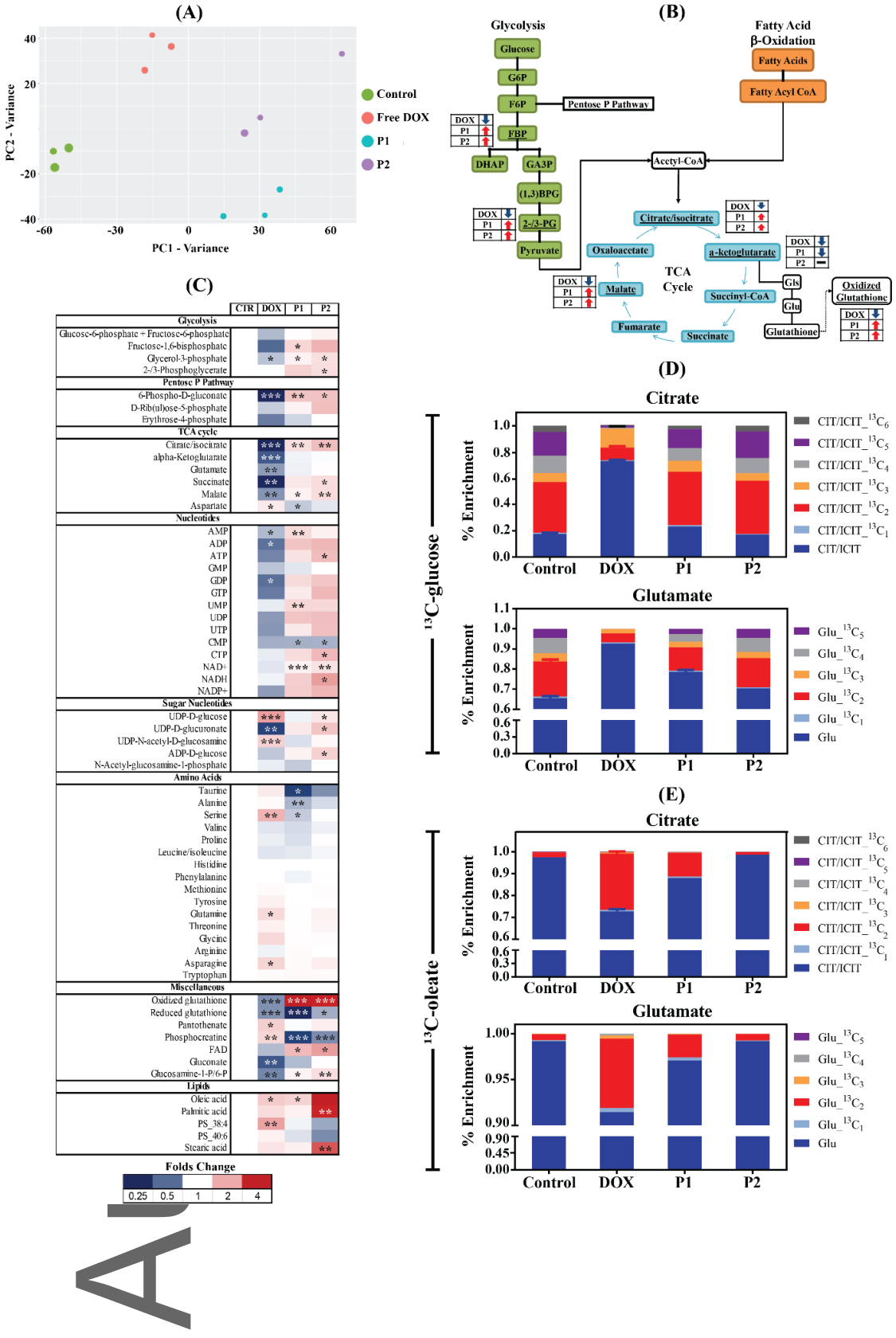

Figure 7. Metabolic response of cells treated by P1/P2 versus free DOX. Untargeted metabolomics analysis and relative flux using stable isotope tracers were used to assess metabolic changes associated with either free DOX or P1/P2 treatment. Targeted analysis shows distinct differences between metabolites of key pathways based on treatment type, as indicated by principle component analysis **(A)**, changes within glycolysis and the TCA cycle **(B)**, and in the heatmap of various metabolic markers **(C)**. Further, using ^{13}C-glucose or ^{13}C-oleate media, we found that free DOX reduces glycolysis while P1 and P2 cause an increase in glycolysis, as shown in the normalized enrichment levels of citrate and glutamate in the presence of U-^{13}C glucose media **(D)**. Results also show that free DOX increases fatty acid oxidation while P1 and P2 have little to no effect on it, as seen by the normalized enrichment of citrate and glutamate in the presence of U-^{13}C oleate media **(E)**. Targeted analysis and flux tracing results are presented as the mean of three replicates ± SEM. Two-tailed Student's t-tests were used to determine the statistical difference between DOX-, P1-, or P2-treated cells compared to untreated (control) cells and are denoted by * for $P<0.05$, ** for $P<0.01$, and *** for $P<0.001$.

***N*-Acetylgalactosamine-targeted, doxorubicin-loaded dendrimer conjugates for hepatic cancer therapy.** Development and in vitro validation of a nanoparticle-based drug delivery method aimed at improving therapy of hepatocellular carcinoma. NAcGal$_\beta$-targeted, doxorubicin-loaded G5 PAMAM dendrimers are synthesized and analyzed for cell-specific delivery and release of the chemotherapeutic drug in hepatic cancer cells. Results show the nano-conjugates offer tunable cytotoxic activity comparable to the free drug, and they induce a unique metabolic response in cancer cells.

polymer-drug nano-conjugates

Sibu P. Kuruvilla, Gopinath Tiruchinapally, Mahmoud ElAzzouny, Charles Burant, Mohamed E.H. ElSayed*

***N*-Acetylgalactosamine-targeted delivery of dendrimer-doxorubicin conjugates influences doxorubicin cytotoxicity and metabolic profile in hepatic cancer cells**

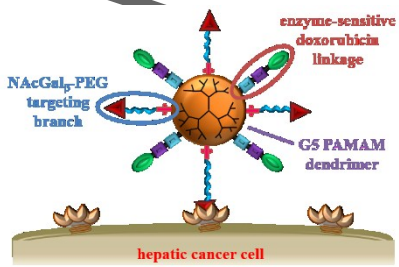

Supporting Information

_N_-Acetylgalactosamine-targeted delivery of dendrimer-doxorubicin conjugates influences doxorubicin cytotoxicity and metabolic profile in hepatic cancer cells

*Sibu P. Kuruvilla, Gopinath Tiruchinapally, Mahmoud ElAzzouny, Charles Burant, Mohamed E.H. ElSayed**

1. Synthesis of NAcGal$_\beta$-PEG*c*-G5-L(x)-DOX Particles:

General Experimental Procedures: All reactions were carried out under nitrogen with anhydrous solvents in flame-dried glassware, unless otherwise noted. All glycosylation reactions were performed in the presence of molecular sieves, which were flame-dried right before the reaction under high vacuum. Solvents were dried using a solvent purification system and used directly without further drying. Chemicals used were reagent grade as supplied except where noted. Analytical thin-layer chromatography was performed using silica gel 60 F254 glass plates. Compound spots were visualized by UV light (254 nm) and by staining with a yellow solution containing $Ce(NH_4)_2(NO_3)_6$ (0.5 g) and $(NH_4)_6Mo_7O_{24}{\cdot}4H_2O$ (24.0 g) in 6% H_2SO_4 (500 mL). Flash column chromatography was performed on silica gel 60 (230–400Mesh). NMR spectra were referenced using Me_4Si (0 ppm), residual $CHCl_3$ (δ ^{1}H-NMR 7.26 ppm, ^{13}C-NMR 77.0 ppm, CD_3OD (δ ^{1}H-NMR 3.30 ppm, ^{13}C-NMR 49.00 ppm, CD_3SOCD_3 (δ ^{1}H-NMR 2.49 ppm, ^{13}C-NMR 39.5 ppm and D_2O (δ ^{1}H-NMR 4.56 ppm). Peak and coupling constant assignments are based on ^{1}H-NMR.

Characterization of anomeric stereochemistry: The stereochemistry of the newly formed glycosidic linkages in N-acetyl galactosamine derivative was determined by $J_{H1,H2}$ through ^{1}H-NMR. Smaller

coupling constants of $J_{H1,H2}$ (below 4 Hz) indicate α linkages and larger coupling constants $J_{H1,H2}$ (6.0 Hz or larger) indicate β linkages.

Mass spectrometry (MS) analysis: ESI-MS measurements were performed according to the published protocols on a Q-TOF Ultima API LC-MS instrument with Waters 2795 Separation Module (Waters Corporation, Milford, MA). All samples passed through an EagleEye HPLC C_{18} column, 3 mm × 150 mm, 5 µm at a flow rate of 0.5 mL/min with a linear gradient from 10% eluent B to 26% eluent B over eight minutes with the column temperature maintained at 45 °C. All injections were performed in the full-loop injection mode using a 10 µL sample loop. Eluent A consisted of a pure aqueous solution and eluent B contained 75% acetonitrile/25% aqueous solution (v/v). The following instrument settings were common for analyses S16 performed in both positive and negative ion modes: source temperature 120 °C, desolvation temperature 400 °C, collision energy 10 eV. When operated in negative ion mode, the mass spectrometer used the following instrument settings: capillary voltage 2.0 kV, cone voltage 35 V, extraction cone 4 V. The following instrumental parameters were used for data acquisition in positive ion mode: capillary voltage 3.5 kV, cone voltage 35 V. Sample concentrations were 1mg/mL. MALDI mass spectra were recorded on a Shimadzu Axima-CFR plus MALDI-TOF. The matrix used was 2,5-dihydroxy-benzoic acid (DHB) and Melittin from honeybee venom (M2272 from Sigma-Aldrich) as the calibration compound.

We have reported the synthesis and analytical data for L3-DOX, L4-DOX linkers and compounds 1-8 in our previous work[18]. Below, we describe the synthesis and analytical data for compounds 9-13.

1.1 N-((2R,3R,4R,5R,6R)-2-(2-(2-(2-aminoethoxy)ethoxy)ethoxy)-4,5-dihydroxy-6-(hydroxymethyl) tetrahydro-2H-pyran-3-yl)acetamide-PEG-NH-Cis-Ac-COOH (**9**):

Compound **8** (0.195 g, 0.074 mmol) was dissolved in MeOH (6 mL) followed by addition of K_2CO_3 (0.102 g, 0.74 mmol), 1 M NaOMe solution (1 mL, pH was adjusted to 9.0-9.7 by drop wise addition) and stirred for 1 h at 0 ^{o}C then for 12 h at room temperature. The reaction solution was gradually acidified by adding ice-cold 1N HCl solution while stirring the mixture at 0 °C till the pH dropped to

3.0. The reaction mixture was dialyzed (MWCO 1kDa) against deionized water for 36 hours and lyophilized to obtain compound **9** as an off-white solid (175 mg) in 94.5% yield.

^{1}H NMR (500 MHz, $CDCl_3$): δ 1.85 (s, 3H, CH_3, OAc), 2.02 (s, 3H, CH_3, OAc), 2.04 (s, 3H, CH_3, OAc), 2.16 (s, 3H, CH_3, OAc), 3.08-3.20 (m, 6H), 3.26-3.44 (m, 4H,*CH_2*-COOH), 3.46-3.56 (m, 8H, $H_{a,b.c.d.e.}$), 3.58-3.3.72 (m, 180H, PEG-H), 3.72-3.86 (m, 4H, $H_{f,}$ $H_{a'}$), 3.94-4.02 (m, 2H, H_a), 4.04-4.16 (m, 3H, H_2, $H_{6,6'}$), 4.32-4.38 (m, 1H, H_3), 4.41 (dd, 1H, *J* = 1.6 & 1.0 Hz, H_5), 5.31 (d, 1H, *J* = 1.6 Hz, H_4), 6.36 (d, 1H, *J* = 6.8 Hz, H_1), 6.78 (s, 1H, olefin), 7.70-7.72 (2bs, 2H, COOH). ESI-MS: $[M+H]^-$ calculated for $C_{14}H_{28}N_2O_8$-PEG-NH-cis-Ac is 2508.30, found 2507.20.

1.2 Dendrimer coupled-4-pentynoic acid to form G5- pent-4-ynamide compound (G5-(alkyne)$_{15}$ or **10**):

Commercially available G5-Dendrimer (0.2 g, 0.00693 mmol) and 1-pentynoic acid (13.6 mg, 0.138 mmol) were dissolved in anhydrous DMSO (7 mL) and added PyBOP (108 mg, 0.208 mmol), DIPEA (base, 0.12 mL, 0.693 mmol) and stirred at RT for 36 h. Reaction mixture was transferred in to dialysis cassette (7KDa) and dialyszed for 2 days followed by lyophilization afforded compound **10**, (0.2 g) in 96% yield.

^{1}H-NMR (500 MHz, D_2O): δ 2.18-2.34 (m, 240H, G5-H), 2.40-2.50 (m, 120H, G5-H), 2.56 (s, 14H, pentyne-H), 2.58-2.74 (m, 290H, 240 G5-H + 50 H from CH_2 of 4-pentynoic acid), 2.97(t, 10H, *J* = 6.0 Hz, pentyne-H), 3.03-3.24 (m, 240H, G5-H), 3.44 (bs, 240H).

MALDI analysis: The molecular weight of parent G5-$(NH_2)_{128}$ is 28, 826, and the molecular weight observed for G5-alkyne is 30,033, which has 1,207 daltons more than its parent dendrimer. This is attributed to alkyne units; each 4-pentynoic acid contributes 81 daltons. Therefore obtained alkyne functionality is 15 units.

1.3 (N-((2R,3R,4R,5R,6R)-2-(2-(2-(2-aminoethoxy)ethoxy)ethoxy)-4,5-dihydroxy-6-(hydroxymethyl)tetrahydro-2H-pyran-3-yl)acetamide-PEG-NH-Cis-Ac)$_{16.6}$-G5-(alkyne)$_{15}$ (**11**):

Compound **9** (112 mg, 0.0449 mmol, 18 eq) was dissolved in 7.5 mL of 0.1 M potassium phosphate buffer (pH 6.0) followed by addition of EDC.HCl (34 mg, 0.178 mmol, 1:4 eq with acid), catalytic amount of HOBt (4 mg) and the reaction mixture was stirred at room temperature for 30 minutes. G5-(alkyne)$_{15}$-(NH$_2$)$_{115}$ dendrimer **10** (75 mg, 0.00249 mmol, 1 eq) was dissolved in 5 mL of MeOH and added to the reaction mixture followed by pH adjustment to 8.0, by drop wise addition of 0.5 M NaOH solution. The reaction mixture was stirred for 36 hours at room temperature before dialyzing (MWCO 10kDa) the reaction solution against deionized water for 36 hours followed by lyophilization to obtain compound **11** as a light orange fluffy solid (140 mg) in 93% yield.

^{1}H NMR (500 MHz, D_2O): δ 1.82-1.88 (m, 31H, CH_3, NHAc), 2.15-2.36 (m, 316H, G5-H, along with other ethylene dioxide protons), 2.40-2.52 (m, 120H, G5-H, un-overlapped G5 protons), 2.54-2.76 (m, G5-H, along with other ethylene dioxide protons), 2.76 (bs, 9H, -OH), 2.82 (bs, 8H, -OH), 2.86 (bs, 27H), 2.92-3.00 (m, 42H), 3.02-3.26 (m, 361H, G5-H, along with other ethylene dioxide protons), 3.26-3.38 (m, 62H), 3.40-3.72 (m, 2795H, PEG-protons); 3.78 (bs 13H), 3.90 (bs 14H), 3.92 (bs 16.4H), 4.20 (bs 12H), 4.36 (bs 14H), 5.42 (d, 12H, *J* = 4.4 Hz), 5.78 (d, 1H, *J* = 7.4 Hz, H_1), 7.22 (bs, NH protons), 7.52 (bs, NH protons), 7.62 (bs, NH protons), 7.94 (bs, NH protons).

NMR analysis: We took un-overlapped G5-protons as standard G5-120 protons at 2.40-2.52 ppm, and we obtained 2795 PEG- protons at3.40-3.72 ppm. Each 2KDa PEG unit contains approximately 172 protons, and then we were able to attach 16.25 *cis*-Ac-PEG-NAcGAL units on to the G5 surface.

MALDI analysis: The molecular weight of the compound **9** is 2508, and compound **10** is 30033. The molecular weight observed for (alkyne)$_{15}$-G5-(cis-Ac-PEG-NAcGAL) is 71,922 which has 41,889 daltons more than its parent dendrimer. This is attributed to *cis*-Ac-PEG-NAcGAL units; each *cis*-Ac-PEG-NAcGAL contributes 2508.2 daltons. Therefore obtained *cis*-Ac-PEG-NAcGAL functionality is 16.6 units.

1.4 (N-((2R,3R,4R,5R,6R)-2-(2-(2-(2-aminoethoxy)ethoxy)ethoxy)-4,5-dihydroxy-6-(hydroxymethyl)tetrahydro-2H-pyran-3-yl)acetamide-PEG-NH-Cis-Ac)$_{16.6}$-G5-(L3-Dox)$_{11.6}$ (**12**):

First Flask: Sodium ascorbate (2 mg g, 0.002 mmol), bathophenonthroline sulfonated sodium salt (SBP, 5.5 mg, 0.002 mmol) and Cu(I) 1 mg, 0.001 mmol) was dissolved THF:H_2O, 1:1= 3 mL) and bubbled the nitrogen for 10 min.

Second Flask: L3-Dox-azide (3.7 mg, 0.0042 mmol) was dissolved in THF and $(N\text{-}Ac\text{-}Gal)_{16.6}$-G5-$(alkyne)_{15}$ (**11**, 0.021 g, 0.00035 mmol) in H_2O and bubbled the nitrogen for 10 min. The catalyst flask was heated to 75 °C for 3-4 min (during this time the solution becomes red in color), cool down to RT, and syringe out the catalyst solution while bubbling the nitrogen and added to L3-dox-azide flask carefully (drop wisely), flushed the nitrogen one more time and closed the flask and covered with aluminum foil and stirred for 48 h. Stirring should be slow and constant around 350 rpm. After 2 days, the reaction mixture was transferred into dialysis cassette (10KDa) and dialyzed for 2 days followed by lyphilization afforded **12**, approximately (19 mL, 1 mg/mL, 19 mg, 77% yield).

^{1}H NMR (500 MHz, CD_3OD + 4 drops of D_2O): δ 0.62-0.82 (m, aliphatic protons), 0.86-1.32 (m, G5-protons), 1.52-1.62 (m, G5-protons), 1.72-2.12 (m, including NHAc protons), 2.26-2.46 (m, G5-H, along with other ethylene dioxide protons), 2.52-2.72 (m, G5-H), 3.40-3.72 (m, G5-protons, PEG-protons merged with CD_3OD peak), 3.78-4.12 (m, G5-H), 6.50-8.80 (m, L3 linker and doxorubicin protons), 9.12 (bs, Doxorubicin protons).

MALDI analysis: The molecular weight of parent particle $(alkyne)_{15}$-G5-$(cis\text{-}Ac\text{-}PEG\text{-}NAcGAL)_{16.6}$ is 71,922. The molecular weight observed for $(alkyne)_{15}$-$(cis\text{-}Ac\text{-}PEG\text{-}NAcGAL)_{16.6}$-G5-L3-DOX is 82,254 which has 10,332 daltons more than its parent dendrimer. This is attributed to L3-DOX units; each L3-DOX contributes 893.2 daltons. Therefore obtained L3-DOX functionality is 11.6 units.

1.5 (N-((2R,3R,4R,5R,6R)-2-(2-(2-(2-aminoethoxy)ethoxy)ethoxy)-4,5-dihydroxy-6-(hydroxymethyl)tetrahydro-2H-pyran-3-yl)acetamide-PEG-NH-Cis-Ac)$_{16.6}$-G5-(L4-Dox)$_{13.4}$ (**13**):

First Flask: Sodium ascorbate (2 mg g, 0.002 mmol), bathophenonthroline sulfonated sodium salt (SBP, 5.5 mg, 0.002 mmol) and Cu(I) 1 mg, 0.001 mmol) was dissolved THF:H_2O, 1:1= 3 mL) and bubbled the nitrogen for 10 min.

Second Flask: L4-Dox-azide (3.8 mg, 0.0042 mmol) was dissolved in THF and $(N\text{-}Ac\text{-}Gal)_{16.6}$-G5-$(alkyne)_{15}$ (**11**, 0.021 g, 0.00035 mmol) in H_2O and bubbled the nitrogen for 10 min. The catalyst flask

was heated to 75 ^{o}C for 3-4 min (during this time the solution becomes red in color), cool down to RT, and syringe out the catalyst solution while bubbling the nitrogen and added to L3-dox-azide flask carefully (drop wisely), flushed the nitrogen one more time and closed the flask and covered with aluminum foil and stirred for 48 h. Stirring should be slow and constant around 350 rpm. After 2 days, the reaction mixture was transferred into dialysis cassette (10KDa) and dialyzed for 2 days followed by lyphilization afforded **13**, approximately (17 mL, 1.25 mg/mL, 21.25 mg) in 85% yield.

^{1}H NMR (500 MHz, CD_3OD + 4 drops of D_2O): δ 0.68-0.88 (m, aliphatic protons), 1.02-1.52 (m, G5-protons), 1.54-1.64 (m, G5-protons), 1.80-2.12 (m, including NHAc protons), 2.14-2.50 (m, G5-H, along with other ethylene dioxide protons), 2.52-2.82 (m, G5-H), 3.40-3.92 (m, G5-protons, PEG-protons merged with CD_3OD peak), 3.92-4.12 (m, G5-H), 6.60-8.50 (m, L3 linker and doxorubicin protons), 9.20 (bs, Doxorubicin protons).

MALDI analysis: The molecular weight of parent particle $(alkyne)_{15}$-G5--$(cis\text{-}Ac\text{-}PEG\text{-}NAcGAL)_{16.6}$ is 71922. The molecular weight observed for $(alkyne)_{15}$-$(cis\text{-}Ac\text{-}PEG\text{-}NAcGAL)_{16.6}$-G5-L4-DOX is 84,313 which has 12,391 daltons more than its parent dendrimer. This is attributed to L4-DOX units; each L4-DOX contributes 923.2 daltons. Therefore obtained L4-DOX functionality is 13.4 units.

References:

1. (a) G. Tiruchinapally, Scott H. Medina, Maxim V. Chevliakov, Yasemin Y. Durmaz, Rachell N. Stender, William D. Ensminger, Donna S. Shewach, and Mohamed E.H. ElSayed, "Targeting hepatic cancer cells with PEGylated dendrimers displaying N-acetylgalactosamine and SP94 peptide ligands", Advanced Healthcare Materials, (**2013**) 2, 1337-1350. (b) S. H. Medina, Maxim V. Chevliakov, Gopinath Tiruchinapally, Yasemin Y. Durmaz, Sibu Kuruvilla, and Mohamed E.H. ElSayed, "Enzyme-activated nanoconjugates for tunable release of chemotherapeutic agents in hepatic cancer cells",Biomaterials, (**2013**) 34, 4655-4666.

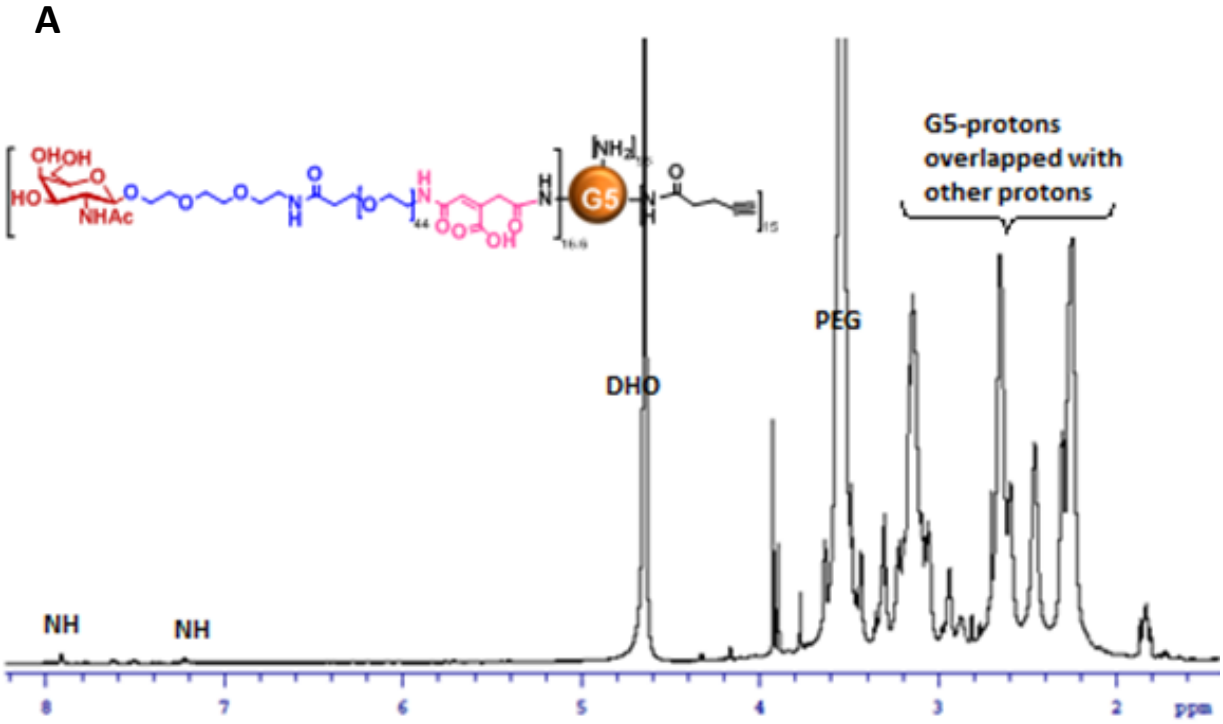

B

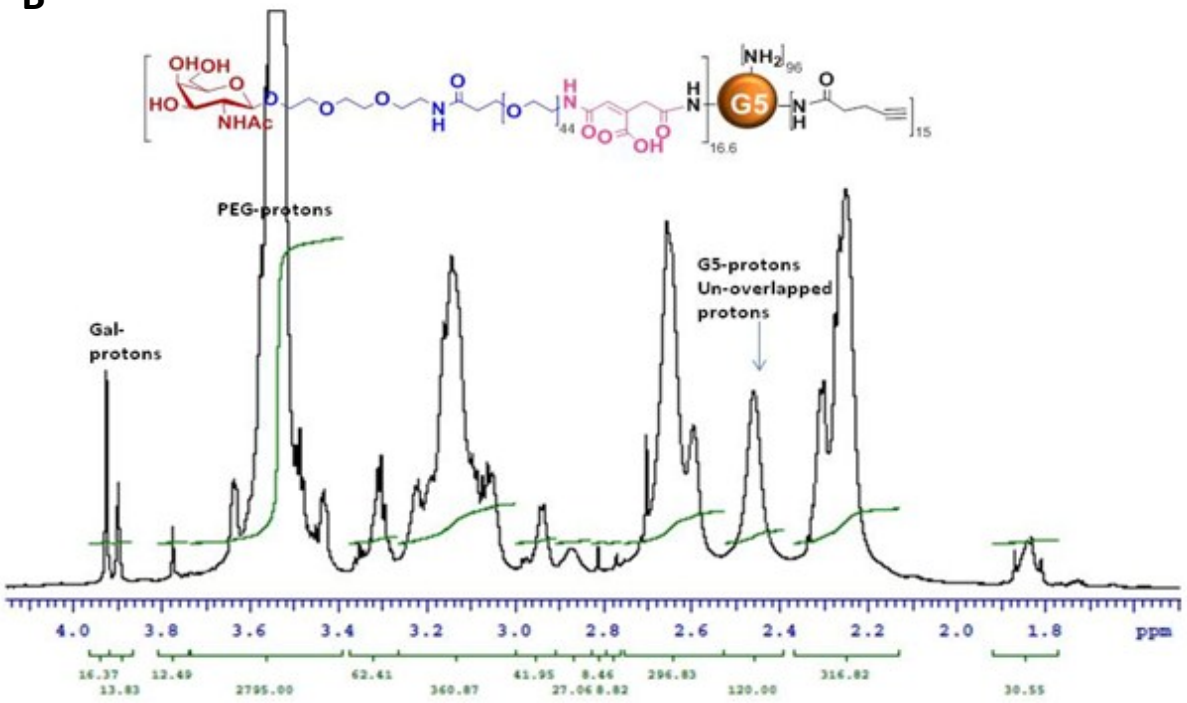

C

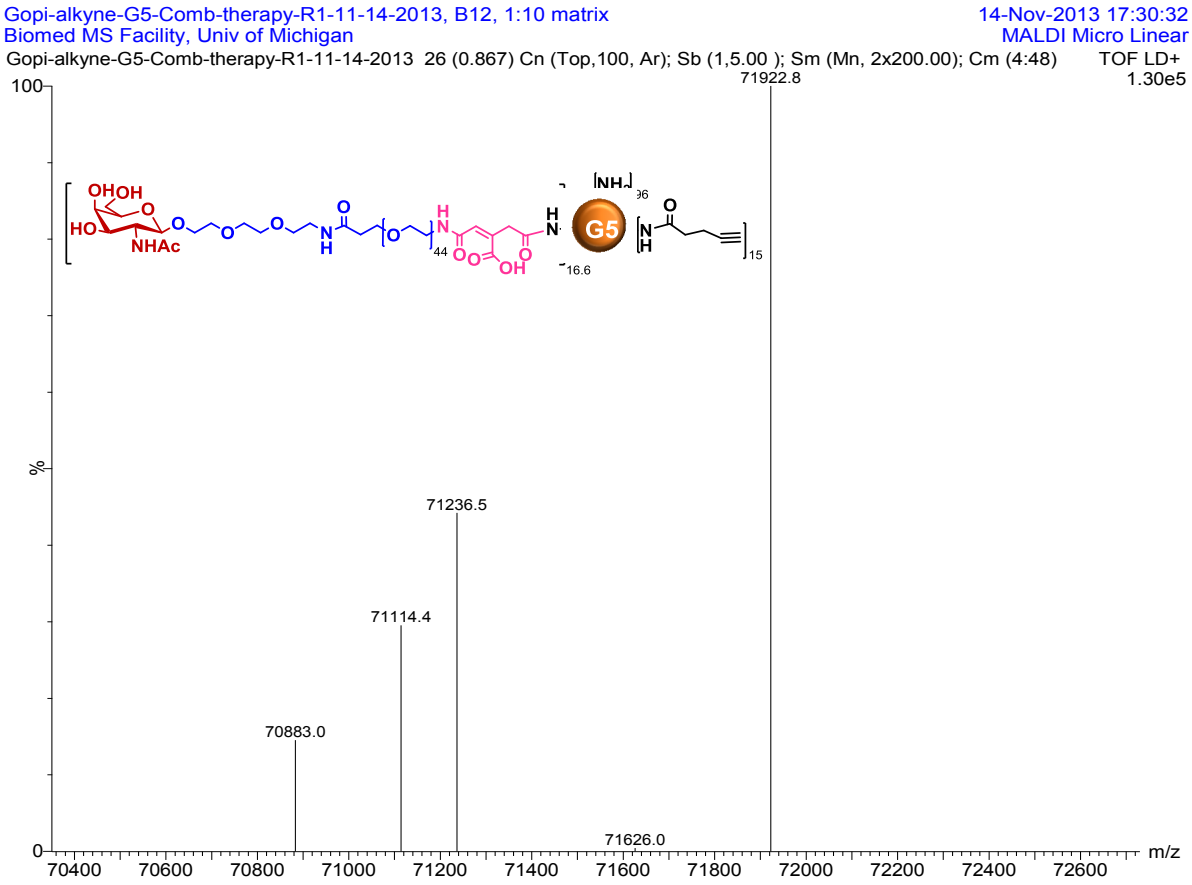

Figure S1.

A: Compound **11** ^{1}H NMR in D_2O, 500 MHz

B: Compound **11** ^{1}H NMR in D_2O (expanded region 0.0-4.0 ppm region)

C: Compound **11** MALDI spectrum:

Analysis:

1. The molecular weight of parent particle G5-(alkyne)$_{15}$ is 30,033.

2. The molecular weight observed for $_m$(NAcGal$_\beta$-PEG*c*)-G5-(alkyne)$_{15}$ is 71,922 which has 41,889 daltons more than its parent dendrimer. This is attributed to NAcGal-PEG*c* units; each

NAcGal-PEG*c* contributes 2508.2 daltons. Therefore the obtained NAcGal-PEG*c* functionality is 16.6 units.

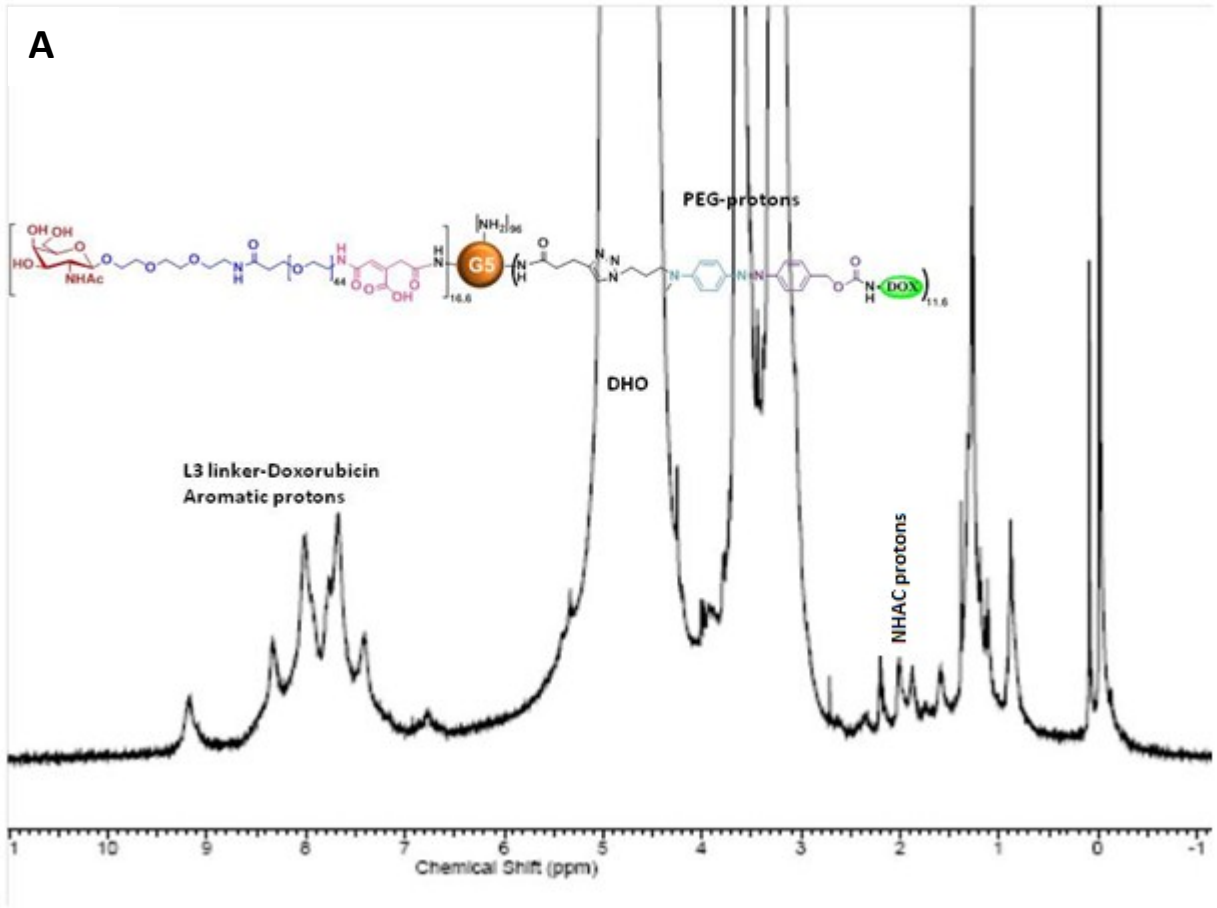

B

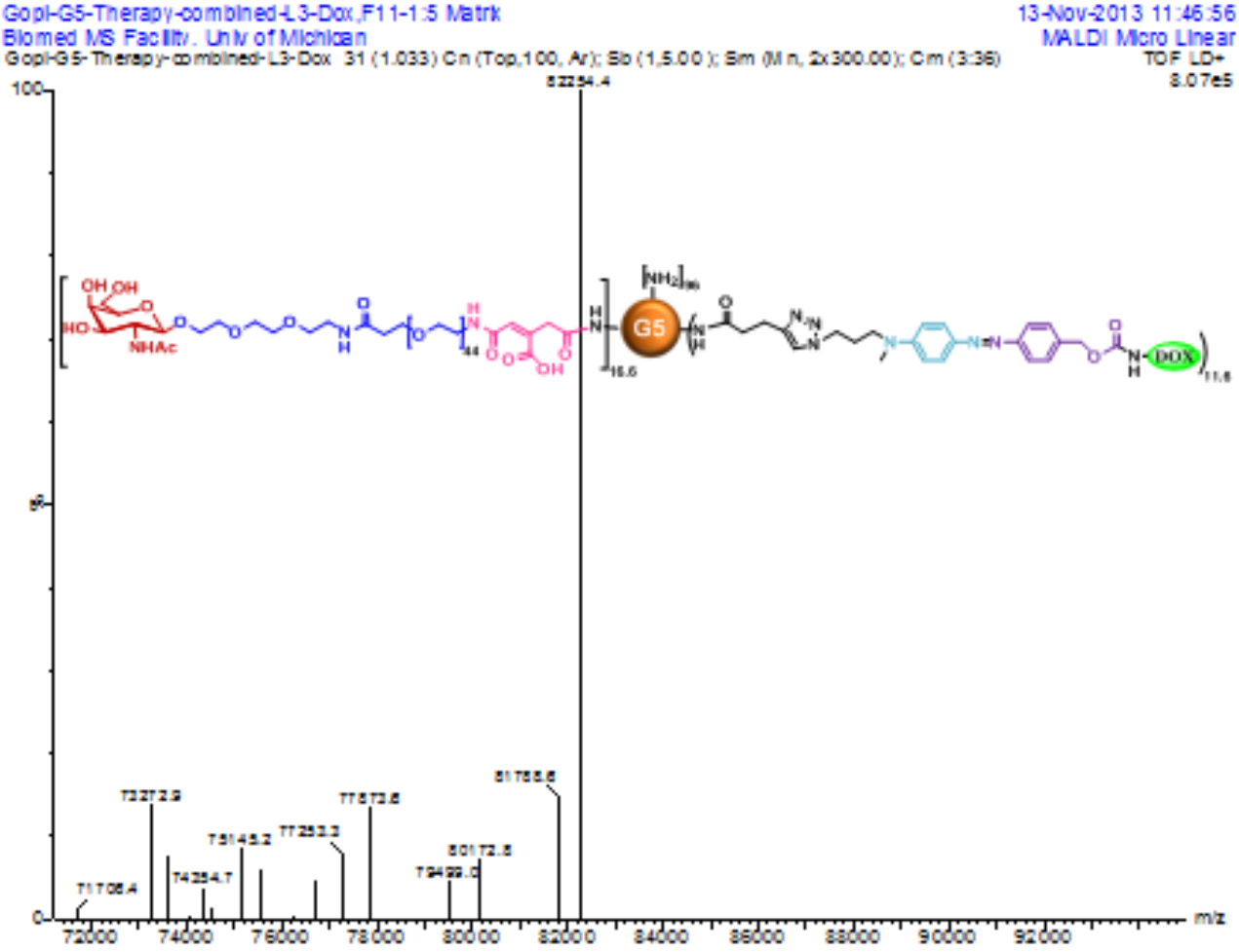

Figure S2.

A: Compound **12** ^{1}H NMR in CD_3OD + 4 drops of D_2O, 500 MHz

B: Compound **12** MALDI spectrum:

Analysis:

1. The molecular weight of parent particle $_{16.6}$(NAcGal$_\beta$-PEG*c*)-G5-(alkyne)$_{15}$ is 71,922.

2. The molecular weight observed for $_{16.6}$(NAcGal$_\beta$-PEG*c*)-G5-L3-DOX is 82,254 which has 10,332 daltons more than its parent dendrimer. This is attributed to L3-DOX units; each L3-DOX contributes 893.2 daltons. Therefore the obtained L3-DOX functionality is 11.6 units.

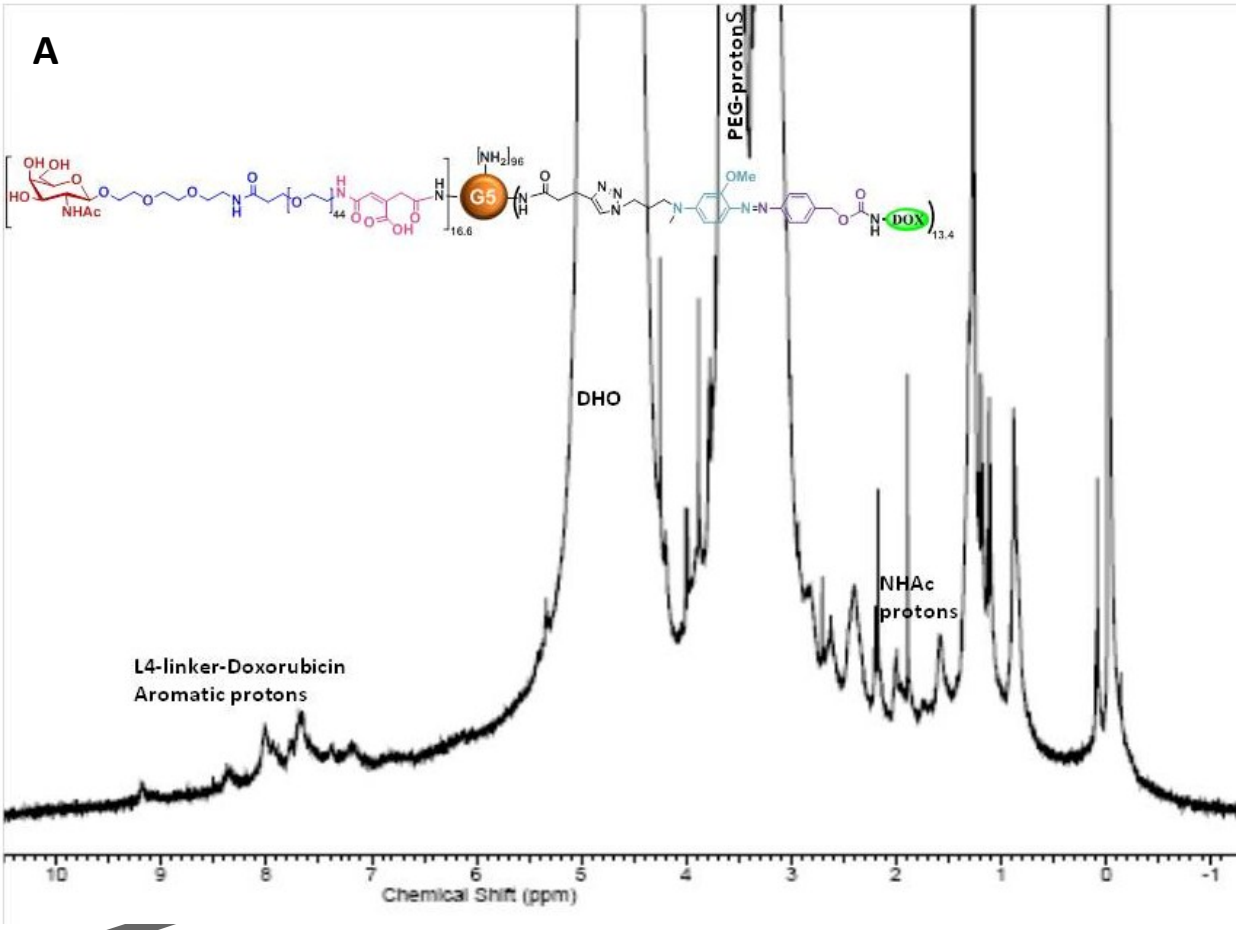

B

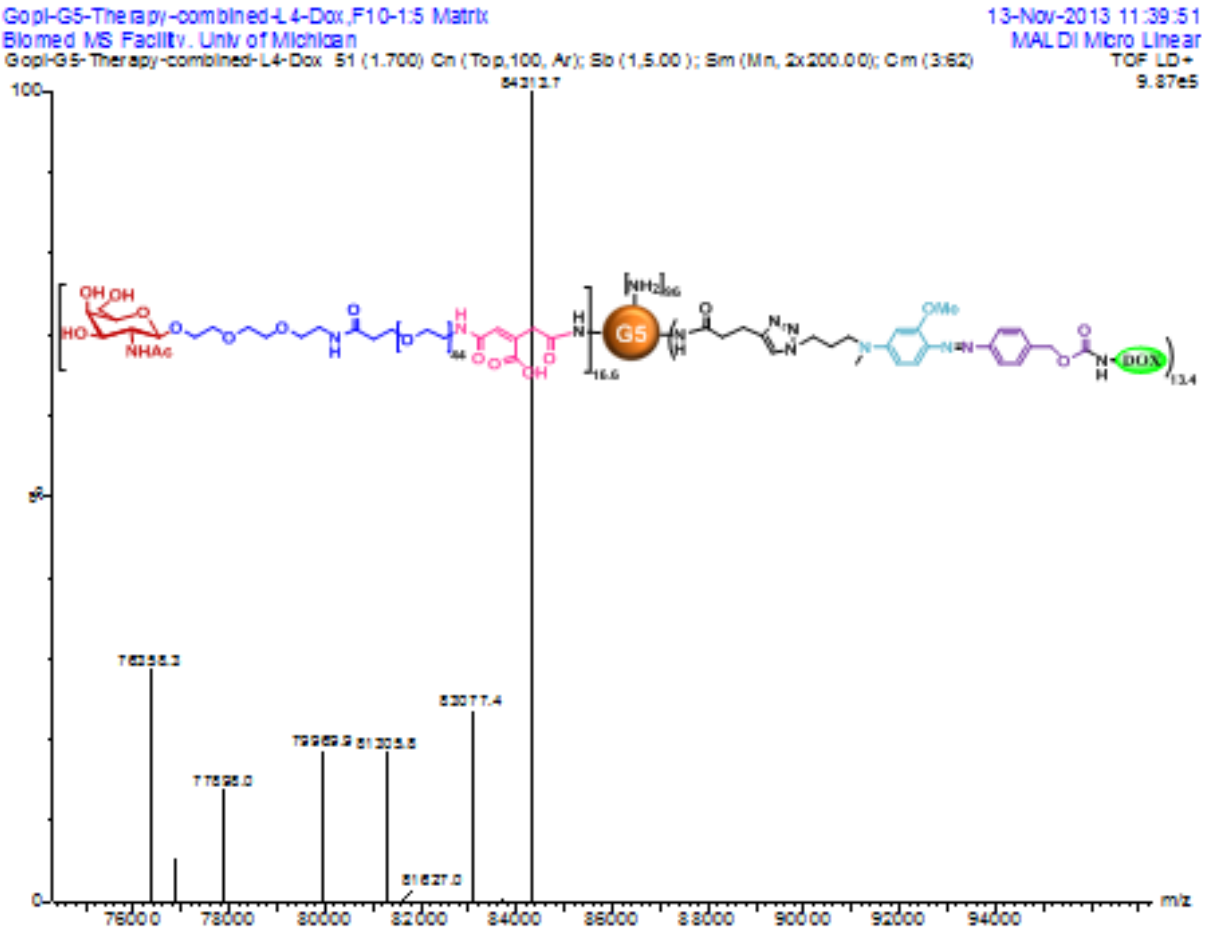

Figure S3.

A: Compound **13** ^{1}H NMR in CD_3OD + 4 drops of D_2O, 500 MHz

B: Compound **13** MALDI spectrum:

Analysis:

1. The molecular weight of parent particle $_{16.6}$(NAcGal$_{\beta}$-PEG*c*)-G5-(alkyne)$_{15}$ is 71922.

2. The molecular weight observed for $_{16.6}$(NAcGal$_{\beta}$-PEG*c*)-G5-L4-DOX is 84,313 which has 12,391 daltons more than its parent dendrimer. This is attributed to L4-DOX units; each L4-DOX contributes 923.2 daltons. Therefore the obtained L4-DOX functionality is 13.4 units

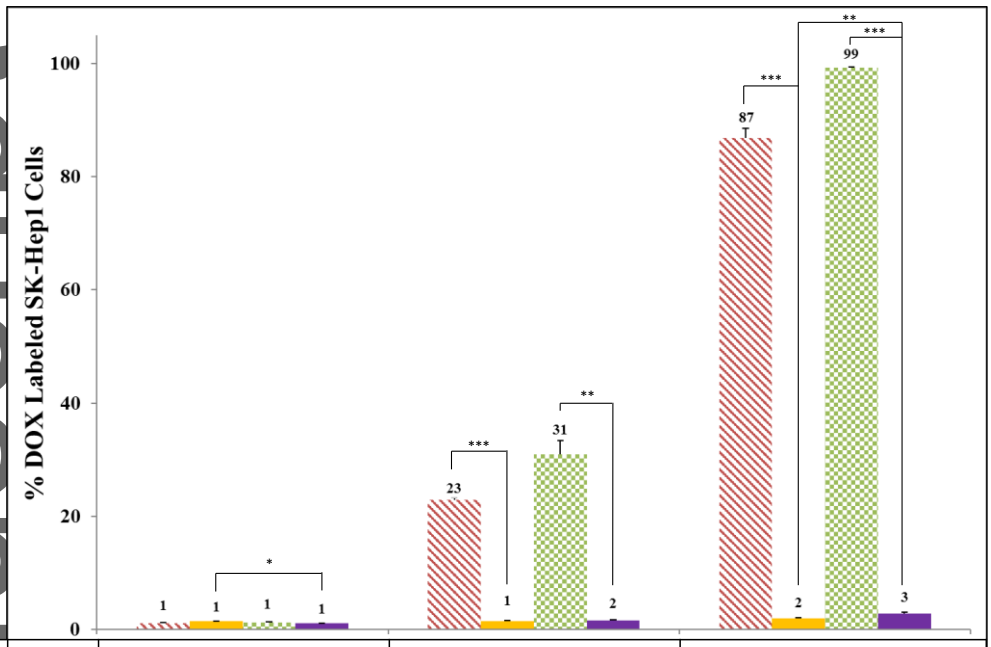

DOX Concentration (nM)	for P1	7.0	349	2795
	for P2	8.1	404	3229
Particle Concentration (nM)		0.6	30	240
NAcGal Concentration (nM)		10	500	4000

Figure S4. Uptake of P1 and P2 particles into a control cell line, SK-Hep1.
SK-Hep1 is known to be an ASGPR-deficient cell line, and flow cytometry results show that P1 and P2 conjugates are not internalized into these cells. Meanwhile, free DOX is internalized in SK-Hep1 cells at similar levels to HepG2 and Hep3B cells, presumably by passive diffusion. These results support that P1 and P2 internalization into HepG2 and Hep3B cells is mediated by the ASGPR. Values are presented as the mean of four replicates ± SEM. A student's t-test was used to compare the statistical significance between different treatment groups, with *P<0.05, **P<0.01, and ***P<0.001.

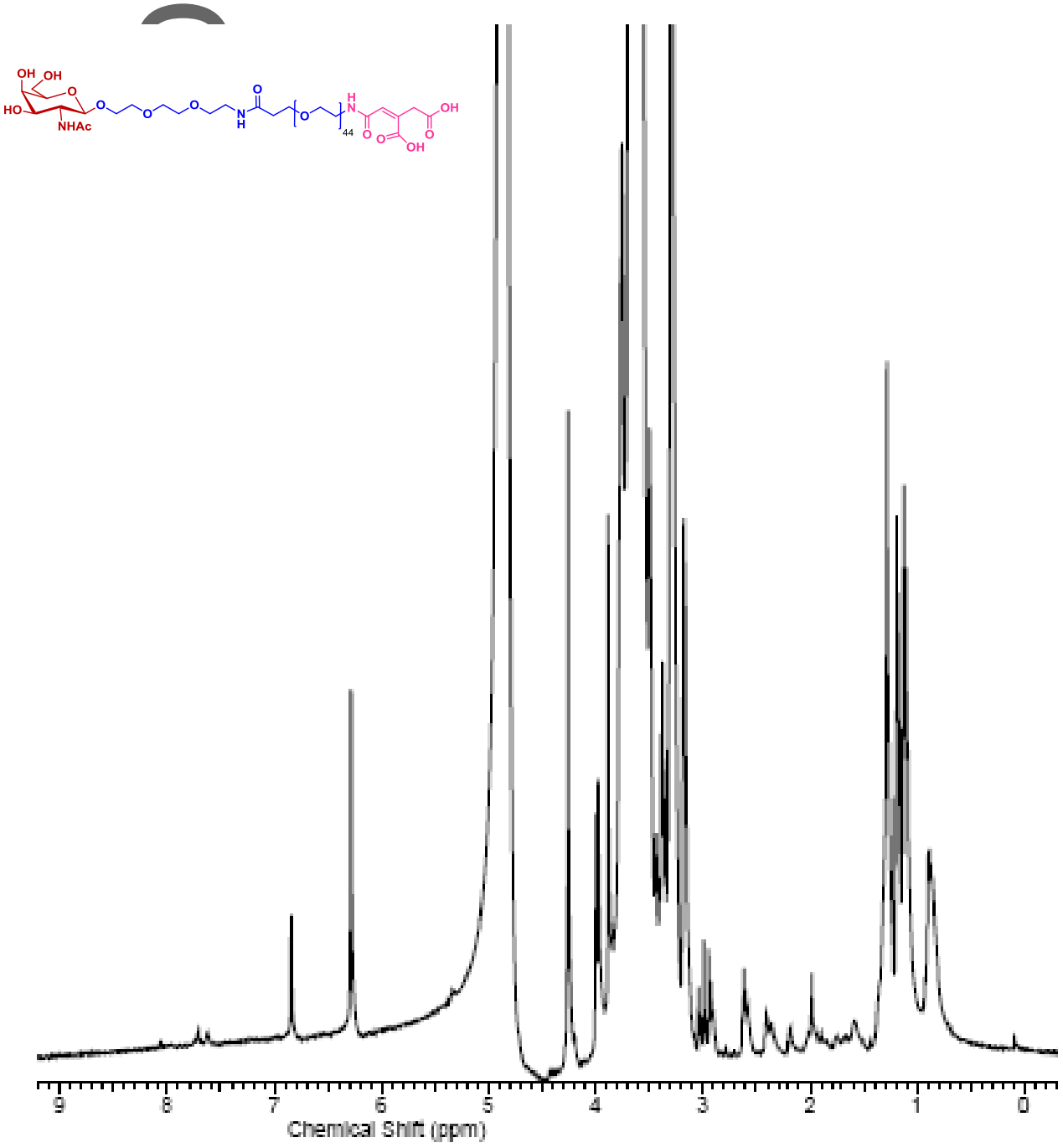

Figure S5. Compound **9** ^{1}H NMR in CD_3OD, 500 MHz

A

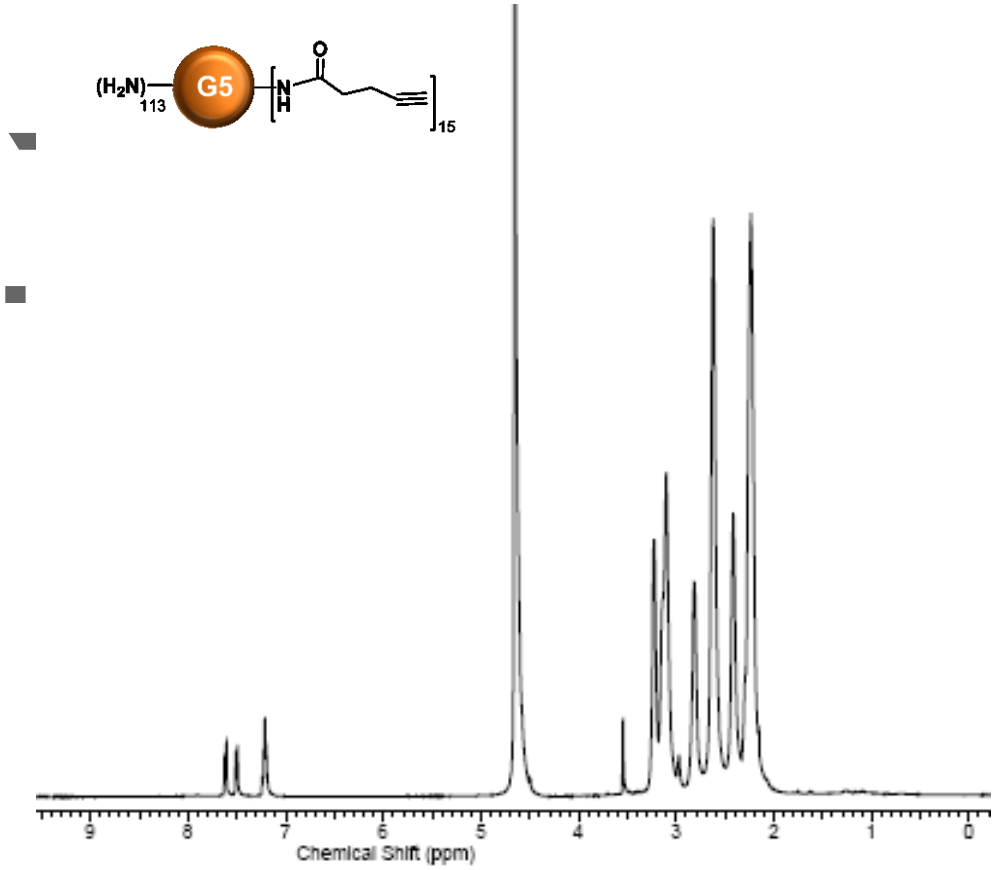

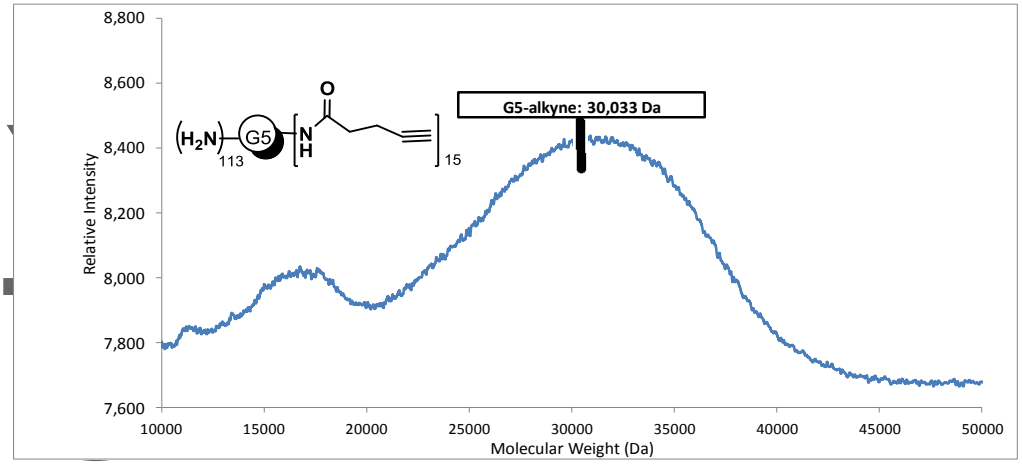

Figure 3.

B

A: Compound **10** ^{1}H NMR in D_2O, 500 MHz.

B: Compound **10** MALDI spectrum:

Analysis:

1. The molecular weight of parent G5-$(NH_2)_{128}$ is 28,826 Da.

2. The molecular weight observed for G5-alkyne is 30,033, which is 1,207 daltons more than its parent dendrimer. This is attributed to alkyne units; each 4-pentynoic acid contributes 81 daltons. Therefore the obtained alkyne functionality is 15 units.